INVESTIGATIONS OF THE ELECTROCHEMICAL CAPACITIVE BEHAVIOUR OF ROOM TEMPERATURE IONIC LIQUIDS

A Thesis Submitted to

The College of Graduate Studies and Research

In Partial Fulfillment of the Requirements

For the Degree of Master of Science

In the Department of Chemistry

University of Saskatchewan, Saskatoon

By:

TYLER R GORE

PERMISSION TO USE

In presenting this thesis in partial fulfillment of the requirements for a Postgraduate Degree from the University of Saskatchewan, I agree that the Libraries of this University may make it freely available for inspection. I further agree that permission for copying of this thesis in any manner, in whole or in part, for scholarly purposes may be granted by the professor or professors who supervised my thesis work or, in their absence, by the Head of the Department or the Dean of the College in which my thesis work was done. It is understood that any copying or publication or use of this thesis or parts thereof for financial gain shall not be allowed without my written permission. It is also understood that due recognition shall be given to me and the University of Saskatchewan in any scholarly use which may be made of any material in my thesis.

Requests for permission to copy or to make other uses of materials in this thesis in whole or in part should be addressed to:

Head of the Department of Chemistry

University of Saskatchewan

Saskatoon, Saskatchewan S7N 5C9

Canada

ABSTRACT

The existence of Room Temperature Ionic Liquids (RTILs) has been known for a long time, but only recently have they been pulled to the forefront of chemical research. This increase in attention can be attributed to a keen interest in their intrinsic properties for a wide variety of potential applications. RTILs have been used as alternative solvents for organic synthesis as well as catalysis, as well as supports for the purification or extraction of metals. Being ionic in nature and liquid at temperatures below 100°C, RTILs lend themselves to the electrochemist. As a result, they have been looked at for use in electrochemical systems such as high capacity batteries and supercapacitors. Due to their extremely high density of charge carriers relative to more well-known aqueous electrochemical systems, a new theoretical approach must be taken. Currently, a large gap exists between theoretical approaches and experimental results. The work contained within this thesis aims to provide insight into the interface between a RTIL and an electrified gold electrode.

ACKNOWLEDGEMENTS

I would like to begin by thanking my supervisor, Dr. Ian J. Burgess, for the countless hours he has spent providing insight, guidance, and above all else patience while I have travelled this long road. I would also like to thank each member of my advisory committee. Dr. Robert W.J. Scott was of great assistance in the synthetic portion of this project. I would like to thank the members of the Burgess group for all of the help that they provided. Specifically, I am grateful to Scott Rosendahl for his tireless patience in teaching me the fine details of practical laboratory electrochemistry.

Research is not possible without funding. My work would not be possible without the financial support of the Department of Chemistry at the University of Saskatchewan, and the National Science and Engineering Research Council of Canada (NSERC).

John Hayes, I owe you a great debt – all of the countless lunch beers and other late night shenanigans over the years are some of my fondest memories from my time at the U of S. Thank you for your humour, encouragement, and above all else friendship.

In the end, I must thank my family for their support, love, and encouragement throughout the length of this project. I would like to personally thank my father, Richard, and my mother, Brenda for everything they have done for me. Even when you both had no idea what I was talking about, you pretended that you did and asked some of the best (and most useful) questions. Thank you.

TABLE OF CONTENTS

CHAPTER 3 – MATERIALS, METHODS, AND EXPERIMENTAL TECHNIQUES

CHAPTER 4 – ELECTROCHEMISTRY COMMUNICATIONS PAPER AND RELATED WORK

LIST OF FIGURES

LIST OF ABBREVIATIONS

AC	Alternating Current
BMIM-OTf	1-butyl-3-methylimidazolium trifluoromethanesulfonate
BMP-N(Tf)$_2$	N,N-butylmethylpyrrolidinium bis(trifluoromethanesulfonyl)imide
BMPyrr-FAP	1-methyl-1-butylpyrrolidinium tris(pentafluoroethyl)trifluorophosphate
C	Capacitor or Capacitance
CCP	Complex Capacitance Plane
CPE	Constant Phase Element
CV	Cyclic Voltammetry
DC	Direct Current
DL	Double Layer
EDL	Electric Double Layer
EIS	Electrochemical Impedance Spectroscopy
EMIM-N(Tf)$_2$	1-ethyl-3-methylimidazolium bis(trifluoromethanesulfonyl)imide
FRA	Frequency Response Analyzer
GCS	Guoy-Chapman-Stern
HPLC	High-Performance Liquid Chromatography
IHP	Inner Helmholtz Plane
MFT	Mean-Field Theory
NMR	Nuclear Magnetic Resonance
OHP	Outer Helmholtz Plane
PZC	Potential of Zero Charge
R	Resistor or Resistance

RMS	Root Mean Square
RTIL	Room Temperature Ionic Liquid
VOC	Volatile Organic Compound

CHAPTER 1

INTRODUCTION

1.1 GENERAL INTRODUCTION TO ROOM-TEMPERATURE IONIC LIQUIDS

Room Temperature Ionic Liquids (RTILs) have been known for a relatively long period of time, but have seen an increased focus in recent literature from a wide variety of researchers – from the organic chemist to the physical chemist. RTILs have been known by a host of different names; "Ionic liquids" and "molten salts" appear to be most common. The variety in nomenclature tends to make literature searching more difficult. The difference between these two terms comes from a historical sense. The term "molten salt" has typically been used to refer to liquid salts at elevated temperatures (above room temperature), while ionic liquid typically refers to those that remain liquid at room temperature. Nomenclature aside, these types of materials are very interesting and attractive to the chemist for their unique properties and wide array of potential applications.

As their name suggests, this class of compound is comprised of a mixture of ions (almost always binary) that maintain a liquid state below the boiling point of water. RTILs typically have no vapour pressure, are very thermally stable, and given their ionic nature are conductive. Electrochemists have been interested in RTILs for a long time as a result of these interesting properties. In and of itself, a RTIL is an electrolyte, but lacks a solvent. This presents a situation not often seen by the electrochemist. Initial research has shown that RTILs can possess a wide potential window within which the RTIL is stable and resists degradation or decomposition. The

potential window has been shown to be in excess of 4 Volts for some RTILs [1]. This property alone presents an opportunity – aqueous based electrochemical systems very rarely exhibit such a wide potential window. As with any new compound or material, practical applications are immediately sought. The list of potential devices, schemes, and ideas for the use of RTILs is extensive. The frontrunners are typically restricted to the suggestions that RTILs can be used as so-called "green" solvents for synthetic reactions, many different types of electronic sensors, and in electronic energy storage devices such as high-capacity batteries and super capacitors. The "green" solvent angle is inherently problematic due to the fact that synthetic procedures for producing RTILs are not overly "green" themselves, using large amounts of volatile organic compound (VOC) solvents. For the energy storage device application, the problem arises in the design of such devices. In order to design a battery or super capacitor that will work as it should and do so in an efficient manner, the interactions between the materials must be understood. A thorough understanding of the interface between a metal conductor and an ionic liquid is paramount to the successful incorporation of ionic liquids into electronic components and devices. Without detailed knowledge of the interfacial behaviour, designing an efficient and functional device would be rather difficult. In the literature, there exist a number of different theoretical approaches that attempt to describe and predict this RTIL-electrode interface. There are also many experimental studies that showcase a wide variety of ionic liquids probed with a handful of electrochemical and spectroscopic techniques. The problem is that there is no clear defining behaviour that bridges the gap between theory and experiment. As with any fundamental study of this nature, extreme caution and care must be taken to minimize the number of variables involved. When one considers the interface between an electrode and electrolyte – be it aqueous, or an RTIL – purity must be considered a top priority. The inclusion of any level of impurity into the so-called

double layer region will alter the response and this effect must be minimized. Prior to the beginning of this thesis work, the vast majority of studies in the literature tended to ignore this and proceeded using commercial samples with minimal treatment, simply quoting the manufacturer's stated purity levels.

Another important parameter of the RTIL-electrode interface is the potential of zero charge, or PZC. This is the potential at which the surface charge density on the electrode is zero. It is fundamentally important potential for any interface – the PZC represents the potential at which the surface changes from positive to negative charge, and *vice-versa*. Theoretically, when the potential is positive of the PZC, the innermost layer will be comprised of negatively charged species, while at potentials negative of the PZC the innermost layer will be made up largely of cations. This is obviously an oversimplification of the situation, but it does help for visualizing the concept of the PZC. This parameter is of striking importance for anyone attempting to design any device based on this interface. Knowing the point at which the surface flips from positive to negative charge will be of key importance to this process. One can imagine that knowing the proper voltage to apply to charge or discharge such a device would be vital.

This thesis focuses on the effort to begin to understand and explain the behavior of an ionic liquid – electrified gold interface by applying previous theoretical work, a proven high-purity synthetic scheme, and modern electrochemical characterization techniques and methods.

1.2 ELECTROCHEMISTRY WITH IONIC LIQUIDS

RTILs present a significantly unique challenge to the modern electrochemist. All of the theories, equations, and models that have been built to help us describe and understand liquid-state electrochemical systems have been based upon dilute electrolytes. Typically, a salt was dissolved in a solvent at low concentration such that the solvent molecules greatly outnumbered the ions or molecules that comprised the electrolyte. Electrochemistry of high concentration electrolytes is uncommon, but not totally non-existent, however it is usually limited to high-temperature molten inorganic salts, such as molten $AlCl_3$ which is used in Aluminum refining. In the late 1990's and early 2000's with the onset of the RTIL in the form that we know it today – both water and air stable organic RTILs have breathed new electrochemical life into the realm of high concentration electrolytes. The major attraction to RTILs over high-temperature molten salts is simply the high temperature requirement of the latter. This type of environment is harsh and not practical for some of the applications envisioned for RTILs.

As mentioned previously, before one can effectively design a device around an RTIL, one must understand how the RTIL behaves within the framework of the device. Thus, a fundamental knowledge of the interaction between the RTIL and an electrified interface must be obtained. As potentially useful as RTILs are, their properties are somewhat problematic for the classically trained electrochemist well-versed in handling and working with an aqueous based electrolyte housed in a typical electrochemical cell. The majority of the common organic RTILs are highly hygroscopic and will rapidly entrain water from the atmosphere. This alone necessitates not only the usual inert atmosphere used with aqueous electrolyte based experimental setups, but also this atmosphere must be water-free and must be maintained as such. Many researchers opt to work within the confined environment of a glove-box, but it is possible to mitigate the potential for water

contamination without such an expensive piece of equipment. Aside from the apparatus itself, the RTIL and electrode surface must be properly prepared, transported, and brought together in such a way to avoid water or other contaminants from entering the cell. These procedures will be discussed in detail in subsequent chapters.

1.2.1 WHY RTILs?

The preceding sections presented a basic summary and background on RTILs, some of their interesting properties, and challenges encountered when working with them. All of this information begs the question – why do we want to examine and work with these types of substances? What is the motivation?

First and foremost, RTILs are as old as they are new. Recently, they have seen a sort of renaissance with synthetic chemists bringing many new air and water stable RTILs to light. As a direct result, ionic liquids are a class of compound that give rise to a great number of ideas for their direct application. Immediately, the need to understand the fundamentals of RTIL electrochemistry is evident.

In a secondary sense, if one were to survey the news headlines over the past decade or more, a trending headline would be our dependence upon fossil fuels for energy and its impact on our environment. As we search for a renewable, clean(er) energy source to satisfy our growing needs we have no doubt turned to looking long and hard at the sun to find a way to efficiently harvest its energy. As the technology of photovoltaics progresses, we will need a way to store this energy. Many have proposed the use of high-density electrolytes such as RTILs in high capacity, high efficiency energy storage devices such as batteries and supercapacitors. This impending

energy crisis itself is a strong motivator to drive the research toward understanding RTILs and how we can put them to use.

1.3 THESIS OBJECTIVE

The intended objective of this research is to explore the world of RTIL electrochemistry in an attempt to help bridge the knowledge gap between theory and experimental results. At the onset of this research, this gap was relatively wide – excellent theoretical work existed but there was an absence of high quality experimental data to validate proposed models. To accomplish such a task, a concentrated effort must be made to ensure that all factors are considered. This includes systematically choosing an RTIL and electrode combination to work with and ensuring the highest level of purity. RTIL handling and processing regimes need to be created to provide a high degree of repeatability. All of these factors contribute to the big picture understanding of the RTIL-electrode interface that is surely needed before attempting to apply the potentially useful RTIL in some form of electronic or electrochemical device.

1.4 THESIS OUTLINE

The work contained within this thesis will start with a review of basic electrochemical interfacial models and why they are problematic with RTILs. It will cover the preexisting research in the literature with a separate focus on both theoretical and experimental work. This thesis will also cover efforts in designing a workable electrochemical cell, and synthesis, handling procedures and purification of the ionic liquid, 1-butyl-3-methylimidazolim trifluoromethanesulfonate

(BMIM-OTf). This thesis will explain the electroanalytical methods used and show a set of published results that encompass our initial investigation of the unique behaviour of BMIM-OTf on a polycrystalline gold surface. It will explore and attempt to provide context and meaning for cyclic voltammetry, chronocapacity, and AC Voltammetry experiments as applied to RTILs. This work was initially published in *Electrochemistry Communications* in 2010. The next portion of work focuses on the use of impedance techniques towards understanding the nature of the double layer capacity. The final portion of this research involves adapting an electrode immersion method in an attempt to uncover the potential of zero charge for this system.

CHAPTER 2

THEORY & LITERATURE REVIEW

2.1 THE ELECTRICAL DOUBLE LAYER

The aim of this chapter is to give an overview of current research and the background theory that provides the basis for the experimental content of this thesis. Electrochemical double layer theory will be covered for classical aqueous electrochemical systems. Its inability to properly describe RTIL systems will be discussed. Furthermore, the importance of the potential of zero charge will be covered alongside a comprehensive review of the current literature related to the behaviour of the RTIL double layer.

2.1.1 ELECTROCHEMICAL DOUBLE LAYER THEORY FOR AQUEOUS SYSTEMS

The foundation of any aqueous electrochemical system is the interface between an electrified surface and the dilute aqueous electrolyte solution. Defining and understanding this interface is paramount to any effort to utilize a given system in any type of application. When a metal surface or electrode is brought into contact with a dilute aqueous electrolyte solution, an electric double layer (EDL) is formed. The term "double layer" (DL) can lead to confusion; it refers to the existence of two layers of charge in two different phases – the surface charge on the metal and the layer of electrolyte counter-ions in solution. This idea of EDL formation was put forward in 1879 by Hermann von Helmholtz [2]. The Helmholtz model is often referred to as the "parallel plate capacitor" model. It involves two parallel "plates" of charge – the free electronic charge on the metal surface is balanced by a layer of counter-ions laying in a single plane directly on the surface of the metal, maintaining electroneutrality over the interface as a whole. This very

small distance is correlated to the order of the molecular size of the electrolyte counter-ions. The surface charge density on the metal is defined as [3]:

$$\sigma_M = \frac{\varepsilon\varepsilon_0}{d} E \tag{2.1}$$

where ε is the dielectric constant of the medium, ε_0 is the permittivity of free space, d is the distance between the "plates" of charge and E is the applied potential or voltage drop across the interface. Then, differential capacitance is defined as [3]:

$$C_d = \frac{\partial \sigma_M}{\partial E} = \frac{\varepsilon\varepsilon_0}{d} \tag{2.2}$$

and immediately the shortcoming of this model becomes clearly evident. The expression for C_d lacks any dependence upon the potential applied or concentration of electrolytes. The result is a constant value for differential capacitance, and has been shown experimentally to be incorrect [3].

In 1910, Gouy and Chapman proposed [4-6] a more sophisticated model to address the inaccuracy of the Helmholtz model. This new model proposed a distribution of charge away from the electrode surface with no layer of counter-ions directly on the surface. This layer is referred to as the diffuse layer, with a distribution of both cations and anions (depending on the polarization of the surface) that diminishes to bulk concentrations as the distance from the electrode is increased. This model changes the capacitance equation by incorporating a distance that is now dependent upon electrode potential and electrolyte concentration. The electrode potential will influence this average distance via electrostatic repulsive or attractive forces. As electrolyte concentration increases, this distance or separation will decrease, resulting in an increased capacitance. Assuming a symmetrical electrolyte at dilute concentration, we can define the surface charge on the metal as:

$$\sigma_M = -\sigma_S = -(8\varepsilon\varepsilon_0 RTC^*)^{1/2} sinh\left(\frac{|z|e\phi_0}{2RT}\right) \quad (2.3)$$

where C^* is the bulk concentration of electrolyte, z is the (signed) charge, e is the charge of the electron, and ϕ_0 is the electrostatic potential of the electrode. Using the definition of C_d in equation 2.2, an expression is obtained that now considers the potential and electrolyte concentration to calculate the differential capacitance. This theory gets much closer to experiment, but only near the potential of zero charge (PZC). At higher electrode polarizations the model deviates from experimental results [3].

In 1924, Stern noticed that at high electrode polarizations the capacitance values predicted by the GC model disagreed with experiment [7]. Gouy-Chapman failed to account for the volume of the ions themselves, ultimately treating them as point charges. Treating the ions as point charges, no restriction was placed on the number of ions to balance the charge in the interfacial region which results in very large C_d values as the electrode potential moves away from the PZC. Stern's modification was a combination of the Helmholtz and Gouy-Chapman models to include a Helmholtz layer directly adsorbed onto the electrode surface followed by a diffuse layer extending out away from the interface, accounting for the finite volume occupied by ions and their solvated shell. A further modification was made by Grahame, which divided the Helmholtz layer into an inner Helmholtz plane (IHP) and an outer Helmholtz plane (OHP) [8]. The inner plane represents those ions directly adsorbed (specific adsorption describes this situation) on the electrode surface, with the outer representing the plane of closest approach of solvated ions. Figure 2.1 illustrates the structure of the GCS model.

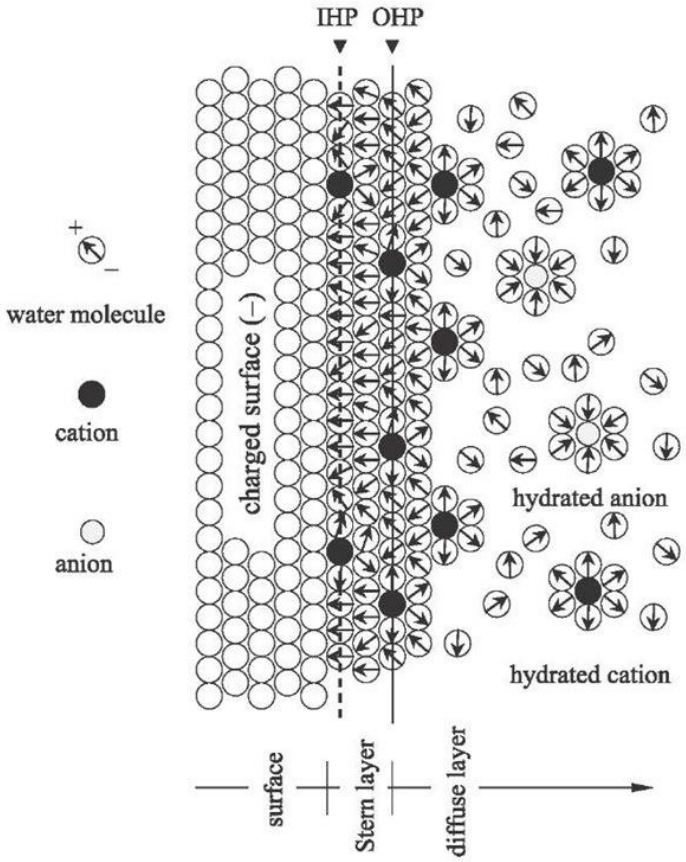

Figure 2.1 – Guoy-Chapman-Stern model of the EDL for classical aqueous based electrochemistry. [74]

The Gouy-Chapman-Stern (GCS) model does very well in predicting experimental results, and has been widely used as the basis for more refined models that more closely match and explain experiment. For this thesis, the most important details to retain from aqueous electrochemistry are; the capacitance is at a ***minimum*** at the potential of zero charge (E_{PZC}), and the above models are based upon the assumption that the electrolyte solution is relatively dilute. The concept and importance of the PZC will be explained in detail in section 2.1.3.

Equivalent circuits play an important role in the analysis of electrochemical systems, as they can be used extensively to describe processes occurring across the interface between the metal

electrode and electrolytes. An equivalent circuit employs combinations of resistors and capacitors wired together in various combinations ranging from simple series configurations to wildly complex arrangements featuring both series and parallel branches. A properly modelled equivalent circuit can very accurately replicate the response of a given electrochemical system. For example, Figure 2.2(a) shows a resistor (R_S) with a capacitor (C_{DL}) wired in series. This equivalent circuit would apply well to a GCS modelled system where a simple charging and discharging of the double layer capacitance works in conjunction with the solution resistance, with no charge actually flowing across the interface [3]. This assumes the application of a DC potential and no specific adsorption of ions directly onto the metal surface. In the case of Figure 2.2(b), a parallel arm exists to account for adsorption kinetics.

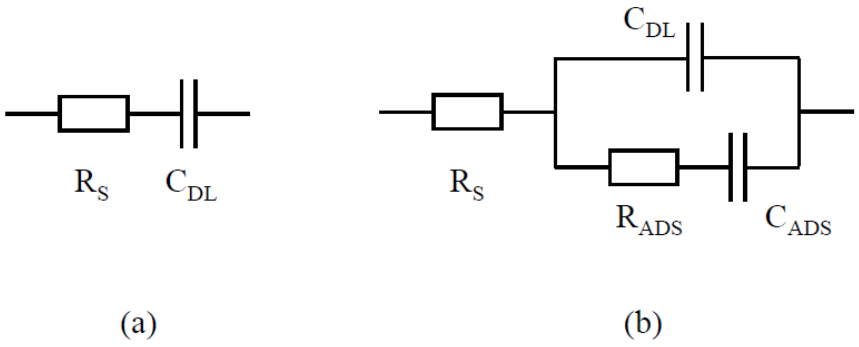

Figure 2.2 – Equivalent circuit models

With experimental data in hand, we can begin to design equivalent circuits to match, and ultimately use fitting routines to back-calculate values for each element of the equivalent circuit. In doing so, the validity of the equivalent circuit can be evaluated. When a circuit's response matches that of the real RTIL system, we can make meaningful conclusions about the interfacial processes based upon the equivalent circuit's individual elements, as well as their values.

Equivalent circuits and how they have been utilized in this research will be further discussed in a later chapter.

2.1.2 ELECTROCHEMICAL DOUBLE LAYER THEORY FOR MOLTEN SALTS AND IONIC LIQUIDS

Considering a RTIL-metal electrode interface is much different than the common aqueous-based electrochemical system discussed previously. The most obvious difference is the departure of a solvent. In a pure RTIL, the only molecules present are ions which immediately breaks the dilute electrolyte concentration requirement of GCS theory, making application of current electrochemical theory incredibly difficult. In order to effectively utilize RTILs and molten salts in novel practical applications, new theories must be developed. Many theoretical chemists have taken to this task via a wide variety of molecular dynamics simulations in an attempt to model a solvent-free interface.

2.1.3 THE POTENTIAL OF ZERO CHARGE

The potential of zero charge is a very important and fundamental property of an electrochemical system and particularly the metal-solution interface. It is such a fundamental parameter because it gives a standard reference point for the interface itself. The point at which the electrode changes from a positive excess surface charge to a negative excess surface charge is referred to as the potential of zero charge or PZC. The condition of the surface can be characterized by knowing on which side of the PZC a certain potential rests. Without any knowledge of where the PZC lies, understanding the condition or status of the surface is difficult. Answering the most

basic of questions – such as whether the surface is positively or negatively charged for a specific potential becomes easy once the PZC is known. It is for this reason that the PZC is an important parameter. With the PZC, we can develop a rational potential range for which the system can safely operate and eliminate the guesswork involved. It is often used as a comparative tool as well as a common bridge between a quantitative measurement and a qualitative description of the interface at this special potential. Understanding where the PZC falls for a given system is paramount to describing the very nature of the different processes occurring at an electrochemical interface. The potential of zero charge is also useful for determining kinetic properties of an interface, and giving information on adsorption and desorption events. The PZC is formally defined as the potential at which the excess charge on the surface of the metal is zero. This is to say that

$$\sigma_M = -\sigma_S = 0 \tag{2.4}$$

which results in a capacitive minimum when this condition is applied. This minimum is correctly predicted in the case of dilute aqueous electrolyte electrochemical systems and verified by experimental results [3]. When looking at the electrochemistry of RTILs, an opposite scenario is encountered. Where one would expect a capacitive minimum at the PZC, a capacitive maximum is observed. As we will see in the next section, this condition is predicted by theoretical work [1, 9-13].

2.2 LITERATURE REVIEW

The literature on RTIL chemistry is vast and expansive. Electrochemical research involving RTILs is no different. Previous work covers two general approaches; theoretical work

using mathematical and computational methods and experimental laboratory work. The most significant theoretical work has been put forth by Alexei Kornyshev, beginning in 2007 and utilizing a simplistic lattice gas model based upon molecular dynamics simulations using mean field theory for a computational basis [9]. This model employs a random distribution of a fixed total number of cations and anions influenced by an electric field sandwiched between two flat boundaries. Since both cations and anions are modeled as 2-D circles of the same size, the lattice can be visualized as a simple grid. Obviously, this model is overly simplistic as an ionic liquid with spherical cation/anion pairs of the same size does not commonly exist in practice. However, the model does provide a base of understanding of the RTIL double layer behaviour. The key feature of the model is that it incorporates a parameter to allow the introduction of voids to potentially accommodate impurities, solvent molecules, or more importantly – to address different levels of packing for different RTILs. The calculations contained within this work result in the appearance of a bell-shaped capacitance plot – deviating from the standard Gouy-Chapman U-shaped capacitance curve seen with aqueous electrochemical systems. To further this new capacitance curve, the calculations include a compacity parameter to quantify the level of free space (or non-RTIL space) within the model. As more voids are introduced into the model, a double hump capacity curve forms with the local minima centred upon the PZC. This curve is often described as “camel-shaped” and can be seen in Figure 2.3 [10].

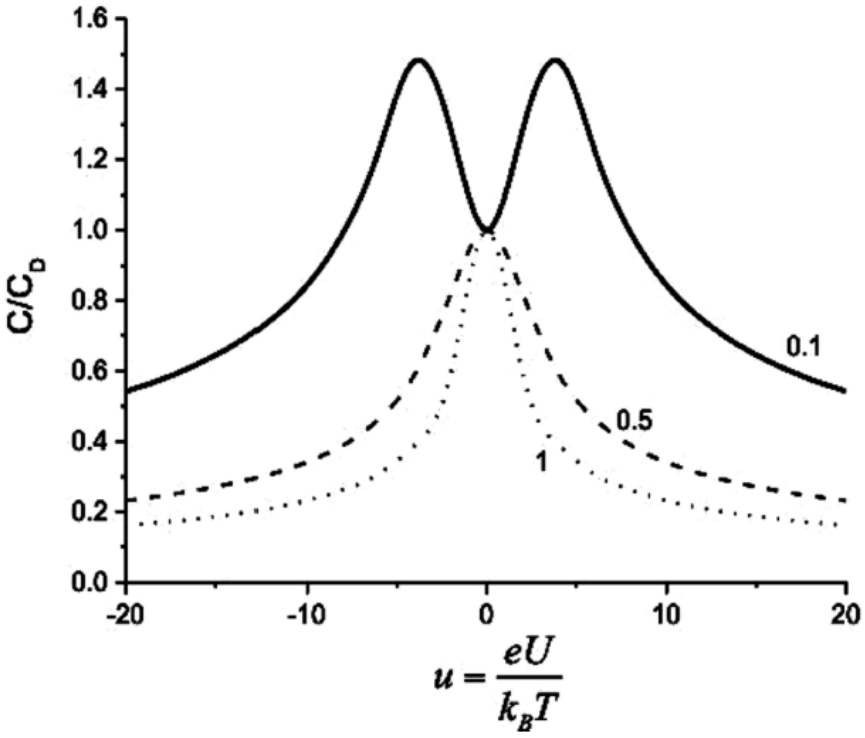

Figure 2.3 – Capacitance curves illustrating the transition from bell-shape to camel-shape with decreasing compacity factor. Reprinted with permission from [10]. Copyright 2014 American Chemical Society.

Fedorov and Kornyshev describe the physical meaning of this transition as simply a packing effect of a reduced density electrolyte [10]. For an ionic liquid, with relatively low level of voids and/or solvent molecules, the electrolyte packs at the surface followed by an expansion of the thickness of the double layer resulting in a decrease in capacity as seen in Figure 2.3.

Moving beyond the MFT approach, the theoretical approaches turned to direct molecular simulations of RTILs at electrified interfaces. This shift was an attempt to address several assumptions and shortcomings of the MFT approach. These new simulation techniques take the next steps by including multibody (or ion-ion) correlations and ion geometry. It was Fedorov and Kornyshev who published the most relevant work in 2008 that introduced the concepts of overscreening and lattice saturation [11, 12].

The concept of overscreening encompasses the idea that a series of layers of cations and anions extend outward from the electrode surface as the potential decays to zero, as the ordering of components returns to neutral or bulk RTIL. Figure 2.4 shows the potential profiles from Fedorov and Kornyshev's simulations [12] at several surface polarizations on two plates held at a simulation distance of 30nm. The purpose of this distance was to ensure that the EDL region of either electrode did not overlap. The effect of overscreening the charge on the electrode is clearly seen in Figure 2.4 – an oscillating decay of layers of opposite sign (charge) extend away from the charged surface out into the bulk. At low polarizations, this overscreening effect is at its strongest. The layers within the EDL over-compensate the charge on the electrode, resulting in an oscillating number of ions in each layer. As the polarization of the electrodes increase, the innermost layer becomes completely filled with tightly packed counter-ions and successive layers are required to fully balance the charge on the electrode. This phenomenon is described as lattice saturation. The authors report that the capacitance data calculated using the simulation data closely resembles the bell-curve predicted by the MFT approach. This makes sense as the situation described requires a thicker EDL, resulting in a reduced capacity.

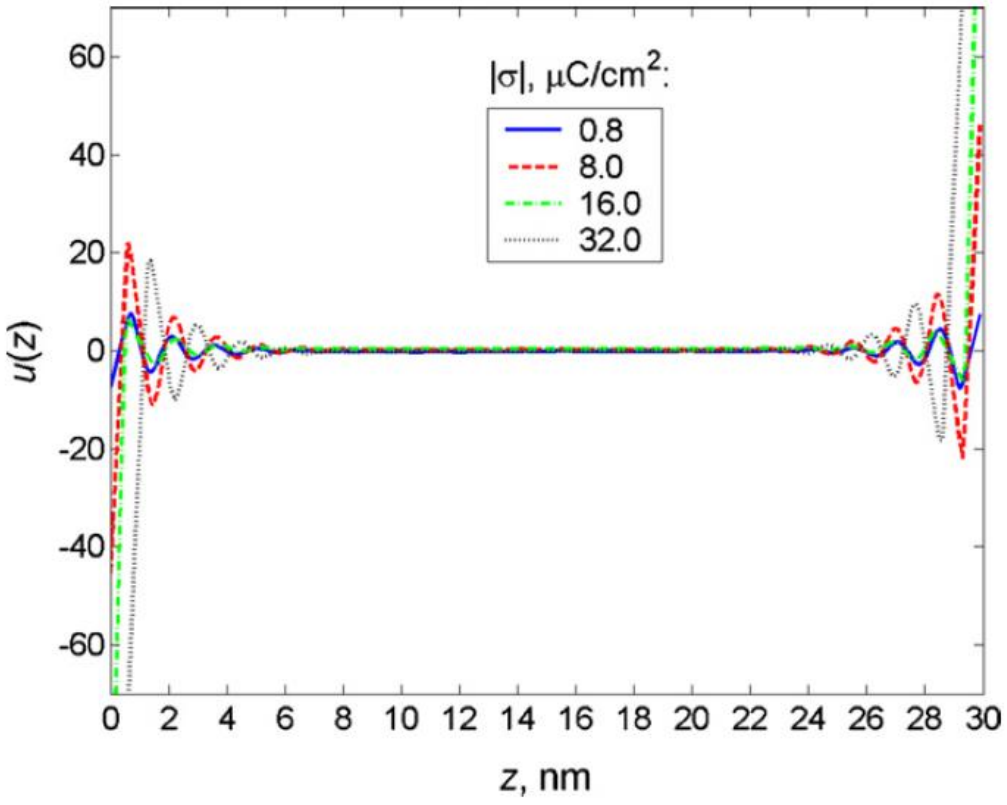

Figure 2.4 – Potential distributions within the simulation box shown at different surface polarizations. Reprinted with permission from [12]. Copyright 2008 American Chemical Society.

The above mentioned work by Kornyshev and Fedorov encompasses cations and anions of identical shape and size. The next step in the progression of the theoretical work is to evolve the modelling of the ions into shapes and sizes that better represent those commonly seen in real world RTILs. To accomplish this, Kornyshev and Fedorov modified the simulations to include three different types of so-called "bead" models [13]. While the anions were kept as spherical beads of identical size, the cations were modelled as multiple bead chains with one bead carrying a positive charge, followed by one or two neutral bead "tails". The introduction of the neutral tails provided a means to incorporate potential voids as well as a way to account for the fatty tails often seen on common RTIL cations. The resulting capacitance curves for the models that incorporated the

neutral beads showed distinct camel-shapes. In addition, the symmetry about the PZC was broken as a result from the ions' size discrepancy. The above overview of work by Fedorov and Kornyshev represents the most thorough treatment of the double layer structure for RTILs. This is not to say that other studies do not exist [14, 15], but this work is the most relevant to this thesis. While these computational treatments of the interface are excellent for providing a visual link between the structure of ions under different potentiodynamic conditions and the resulting capacitance curves, they do not address the real world use and application of RTILs. In order to develop new applications of ionic liquids in electrochemical situations, there is a need to test and verify the model with experiment.

Experimental literature covering the EDL capacitance behaviour of RTILs is relatively new. The wide range of studies utilizing a great array of different RTILs presents a large number of different analyses and conclusions regarding the data. The following section is an overview of the literature regarding experimental work on the capacitive behavior of RTILs.

The body of work by Ohsaka *et al* covers a systematic approach to classifying RTIL electrochemical behaviour and properties [16-22]. Of particular interest is ref. 19, in which an array of popular RTILs were used on selected electrode materials in capacitance studies. The electrodes used in the study included Pt, Au, conductive carbon, and mercury drop electrodes. Their resulting capacitance curves showed two of the predicted shapes, a bell-shaped curve, and a camel-shaped "double-hump" curve. Not only does Ohsaka report different shaped curves for different RTILs, but also that the shape of the curve is largely dependent upon the electrode material. For one particular RTIL, bell-shaped curves were reported on both platinum and gold electrodes, while a camel-shaped curve was observed on a glassy carbon electrode. This indicates that the electrode selection and morphology plays an important role in the shape of the capacitance

response of a particular RTIL. In order to define the processes that are ultimately responsible for these differing capacitance curves, the solid side of the interface must be considered.

Ohsaka's group was not the only one to engage in a systematic study of multiple ILs in the electrochemical arena. The group of Lockett also reported approaching this interface using multiple RTILs [23]. Their results were fairly similar, with RTIL capacitance curves showing the camel shape. Based on the theory provided previously, one would expect this result as they specifically chose RTILs with differing cation and anion sizes. This study, while focusing on three variants of a methylimidazolium chloride IL, sticks to a single electrode – glassy carbon (GC). In the 2008 paper, Lockett describes the congruence of their experimental curves with Kornyshev's MFT calculations. A second, similar report was published in 2010 and addressed criticism by the Ohsaka group regarding the validity of the use of non-metallic electrodes [24]. Lockett tackles this criticism stating that semi-conducting electrodes are valid based on the consistentency of measurements on GC electrodes matching up almost identically to those taken with metallic electrodes.

In 2011, Pajkossy and Kolb published a paper focused on measurements of the capacitive nature of RTIL interfaces with emphasis on the use of high resolution current scales [27]. The authors comment that the majority of RTIL based studies employ current measurements on the milli-amp scale as opposed to the micro-amp scale (all currents normalized with the electrode area). They argue that relevant features are missed with the lower resolution scans, and thus the data should be examined carefully. Since extracting capacitance values from equivalent circuit modelling of EIS data is a common interface analysis tool, care must be taken when fitting to data that was collected on a low-resolution current scale. This insight is an important point to take into consideration when looking at the majority of RTIL electrochemistry based studies. A great

number of these papers show cyclic voltammograms (CV's) over a wide potential window with a current range set far too large to catch the fine structural features of these measurements. This conclusion is one that warranted experimentation. Work began with BMIM-OTf on polycrystalline gold at about the same time as Pajkossy and Kolb's paper was published. The same conclusion was drawn while investigating the safe applied potential window for our RTIL system. On a milli-amp current scale, the CV shows minimal features until the extreme ends of the potential range were reached. As the current increases exponentially at these extreme potentials, a Faradaic process is likely taking place; resulting in damage to the RTIL that results in the creation of impurities. When the current scale is reduced, the CV takes on a new shape that has features not seen in previous CV's (see Figures 4.1 and 4.2). This conclusion that Pajkossy and Kolb mention in their paper is very important due to the wide variety of experimental studies in the literature.

Not only does this array of work contain a mixed variety of RTILs, but also a number of different electrode materials and configurations. All of these combinations make for a very muddled situation in conjunction with the possibility of inaccurate current measurements. The introduction of Electrochemical Impedance Spectroscopy (EIS) data only increases the complexity of the analysis of the interface (A detailed summary of EIS is covered in section 3.2.4). Since EIS measurements extract data from the frequency domain and allow processes with different time scales to be probed, the most often used method of analysis uses equivalent circuit modelling. With a well thought out equivalent circuit, a fitting routine can be used to mathematically extract individual parameters for each element in the circuit. All of these factors make analysis of existing experimental data very difficult given that most equivalent circuit models incorporate the constant phase element (CPE). Pajkossy and Kolb state that the CPE is excellent for reconciling the

deviations from perfect capacitance, but is near impossible to directly extract the value of the capacity or define the real physical meaning of its fitting parameters.

These effects are seen in a 2010 paper by Gnahm, Pajkossy, and Kolb [28], where they study a hexafluorophosphate version of the 1-butyl-3-methylimidazolium RTIL on a Au (1 0 0) surface. They fit the impedance data with an equivalent circuit that is comprised of a resistor (to model solution resistance and diffusion related kinetics) in series with a capacitor and CPE in parallel. The capacitor is referred to as C_{HF}, and corresponds to the double layer capacitance. The meaning of the CPE is difficult to work out in practical terms. If the CPE exponent shows significant deviations from unity, its fitted values can only be reliably used as a relative measure. Based on the authors' analysis, the double layer capacitance is fairly constant over the potential window, while the CPE coefficient exhibits a significant peak that they attribute to the switching of the surface charge sign from positive to negative and *vice-versa*. Kolb and Pajkossy combine the impedance fitting results with a basic immersion experiment that shows the PZC at approximately the same potential as the CPE coefficient maxima. The rational explanation of this behaviour is that a radical, yet slow, rearrangement of the double layer takes place at this zero-crossing potential.

Drüschler, Huber, and Roling published a series of impedance based studies [29-31, 33, 34] using several RTILs, 1-methyl-1-butylpyrrolidinium tris(pentafluoroethyl)trifluorophosphate (BMPyrr-FAP) [33, 34] and another study using two RTILs with a common anion: 1-ethyl-3-methylimidazolium bis(trifluoromethanesulfonyl)imide (EMIM-N$(Tf)_2$), and N,N-butylmethylpyrrolidinium bis(trifluoromethanesulfonyl)imide (BMP-N$(Tf)_2$) [29]. These studies used two different electrode materials, polycrystalline Pt and Au (1 1 1). The most significant of their results come as a result of their treatment of the impedance data. Using an empirical Cole-

Cole type equation to process the complex impedance data into the complex capacitance plane (CCP), the authors were able to resolve two distinct capacitive processes taking place on different time scales, as well as the onset of a third ultra-slow process. This approach differs from the common approach of using an equivalent circuit, as it removes the ambiguity of attempting to rationally design and configure an equivalent circuit. Instead, this method allows the data to resolve the separate processes itself, based upon the timescale. This is an important feature. Not only are the individual timescales visually evident, they do not rely on an equivalent circuit configuration based upon assumptions of the researcher. This method of analysis will be discussed further in conjunction with the collected experimental data and subsequent analysis.

In summary, the literature is full of both theoretical and experimental work regarding the RTIL-metal interface. The theoretical attempts have given excellent context and a new way of thinking about this different type of electrochemical system. Experimentally, the data appears to differ significantly with capacitance curves showing several different shapes, some as predicted by theory, some not. These studies also employ a wide variety of ionic liquids, electrode surfaces and materials that only complicate matters. When studying an electrochemical interface, it is important to pay close attention to all parties involved – both the solid and liquid side must be treated properly and of as high a purity as possible. The majority of studies in the literature take care to use a high quality and well defined electrode, but most fail to go into much detail regarding the RTIL and its level of purity. Most studies use commercial RTILs, and simply quote the manufacturer's purity standards, which are typically less than 10ppm in both water and halides (usually a part of the synthetic process). It is this author's opinion that a higher degree of care must be taken regarding RTIL purity. This position is based on the fact that 10ppm is still a significant concentration on impurity when it comes to investigating an interface using sensitive

electrochemical techniques. To support this, Figure 3.1 shows 3 RTILs at different stages of purification in our lab. Other commercial examples we have seen have ranged from yellow to dark brown and thus, care must be taken when using commercial examples and their resulting datasets.

CHAPTER 3

MATERIALS, METHODS, AND EXPERIMENTAL TECHNIQUES

The goal of this chapter is to cover the experimental details of the research upon which this thesis is based. It will cover the details of how the ionic liquids were synthesized, their purification, and experimental handling and storage requirements. This chapter will also delve into the details of the experimental techniques used as well as the design and construction of custom electrochemical cells for use with RTILs.

3.1 RTIL Synthesis, Purification and Handling Requirements

3.1.1 RTIL Synthesis

The study of electrochemical systems and the measurements involved are inherently sensitive to impurities. As a result of this sensitivity, the ionic liquid required for this research needed to be of the highest purity achievable. Commercially available ionic liquids tend to be of questionable purity and would require a large degree of purification to be successfully used in fundamental studies of their electrochemical properties. Quantifying the level of purity is somewhat difficult, however it was found that the visual clarity and colour of the ionic liquid is generally a good indicator of relative purity [35]. For example, commercial samples of imidazole ionic liquids have been known to be coloured and range from slightly yellow to dark reddish brown. The ionic liquid that was synthesized in this research remained colourless, indicating that the level of purity is very high. Producing 1-butyl-3-methylimidazolium triflate (BMIM-OTf) is

achieved via an ion exchange with the precursor ionic liquid 1-butyl-3-methylimidazolium chloride (BMIM-Cl).

Synthesis of BMIM-Cl is a relatively simple procedure adapted from modifications by R.W.J. Scott and P. Dash on the original scheme by Huddleston [36]. The reagents must be of the highest available purity and were further purified before use. HPLC grade 1-Chlorobutane (Alfa-Aesar) was first distilled under nitrogen using P_2O_5 as a drying agent. 1-methylimidazole (Alfa-Aesar) was distilled under vacuum with NaOH as a drying agent. High purity toluene was obtained from a solvent purification system. The reagents were added (1-chlorobutane in a 10% excess) to a round bottomed flask under nitrogen with a reflux condenser attached. With stirring, the reaction was heated to 75ºC for 72 hours. After 12 hours, a bilayer formed. The top phase contains toluene and unreacted starting materials which can then be decanted and discarded. The bottom phase containing BMIM-Cl, was stirred with an equal volume of HPLC-grade ethyl acetate and stirred for an hour. Using a separatory funnel, the two phases were separated again. Washing with ethyl acetate was repeated several times to remove any unreacted starting material from the BMIM-Cl. At room temperature, BMIM-Cl is a solid, so quite often the separatory funnel had to be heated to prevent crystals from forming. Any remaining ethyl acetate can be removed with gentle heating under vacuum. The IL is then mixed with an equal volume of HPLC-grade acetone and either seeded with a crystal from a previous batch, or chilled to induce crystallization. Excess acetone can be decanted, and the IL can be recrystallized several times to remove any remaining coloured impurities.

To obtain the trifluoromethanesulfonate anion IL (BMIM-OTf), an ion exchange using trifluoromethanesulfonic (triflic) acid is required. The BMIM-Cl is first dissolved in ultrapure Milli-Q (18.2MΩ) water and chilled in an ice bath with stirring. The triflic acid is added drop wise

in a 10% mole excess. This mixture is then stirred for approximately 12 hours, after which an equal volume of HPLC-grade dichloromethane was added to the mixture to form a bilayer. This solution was stirred for another 2 hours and allowed to settle and separate. The top layer which contains water and HCl impurities is decanted and discarded. The bottom layer is then washed with ultrapure Milli-Q water until the washings have a neutral pH, indicating that remaining acid impurities have been removed. It should be noted that the final yield can be increased by further extracting IL from the water washings with dichloromethane. The dichloromethane was then removed under vacuum and slight heating on a rotary evaporator and followed by heating under high vacuum. The resulting ionic liquid was clear and colourless. The IL is extremely hygroscopic and will pick up water from the atmosphere rapidly but can be dried under vacuum and heating to 75ºC for several hours. The IL was not characterized directly but this procedure follows that of Dr. R.W.J. Scott's research group [35].

3.1.2 Purification

High quality electrochemical data requires stringently pure RTIL. Several approaches to further purification following the synthesis were taken including recrystallization of BMIM-Cl, charcoal filtration, and storage over molecular sieves. Given that all commercial samples appeared to have at best a yellowish hue, and at worst a very dark brown colour, we concluded that our colourless BMIM-OTf was indeed of high purity. Beyond the visual analysis, the data from cyclic voltammetry experiments (CV) were a good indication of relative purity across multiple syntheses. When scanned over a wide potential range, minimal features on the CV indicated a high level of purity. This simple method allowed for quick assessment of sample purity between different

experiments. When molecular sieves were used in an attempt to remove impurities we saw an increase in features in the CV data which indicated an increase in the level of impurity. Activated charcoal filtration (by gravity) provided better results, both visually and electrochemically. We were able to remove coloured impurities using activated charcoal which resulted in a colourless BMIM-OTf ionic liquid exhibiting reduced CV peaks within the ~4V potential window. Investigations into the identity of the unknown impurities were never undertaken. The research group headed by Dr. Robert Scott did perform NMR measurements on their RTILs produced using the same synthetic procedure with no direct impurity identification [37]. For a given volume of RTIL, the low level concentration of any impurity relative to the massive concentrations of the cation/anion pair will make them very difficult to detect. Furthermore, the likely impurities will be derivatives of the cation or anion and will have similar chemical signatures that will likely be hidden within the signals for the pure RTIL components. The likely impurities would be remaining unreacted reagents or side-reactions related to the acidic nature of the proton between the two nitrogen atoms on the imidazolium ring. With these reasons and the simple visual and electrochemical tests we performed following a careful synthesis, we concluded that our BMIM-OTf samples were of an extremely high level of purity and thus suitable for use in experiments. See the photograph in Figure 3.1 for a visual comparison of RTIL purity.

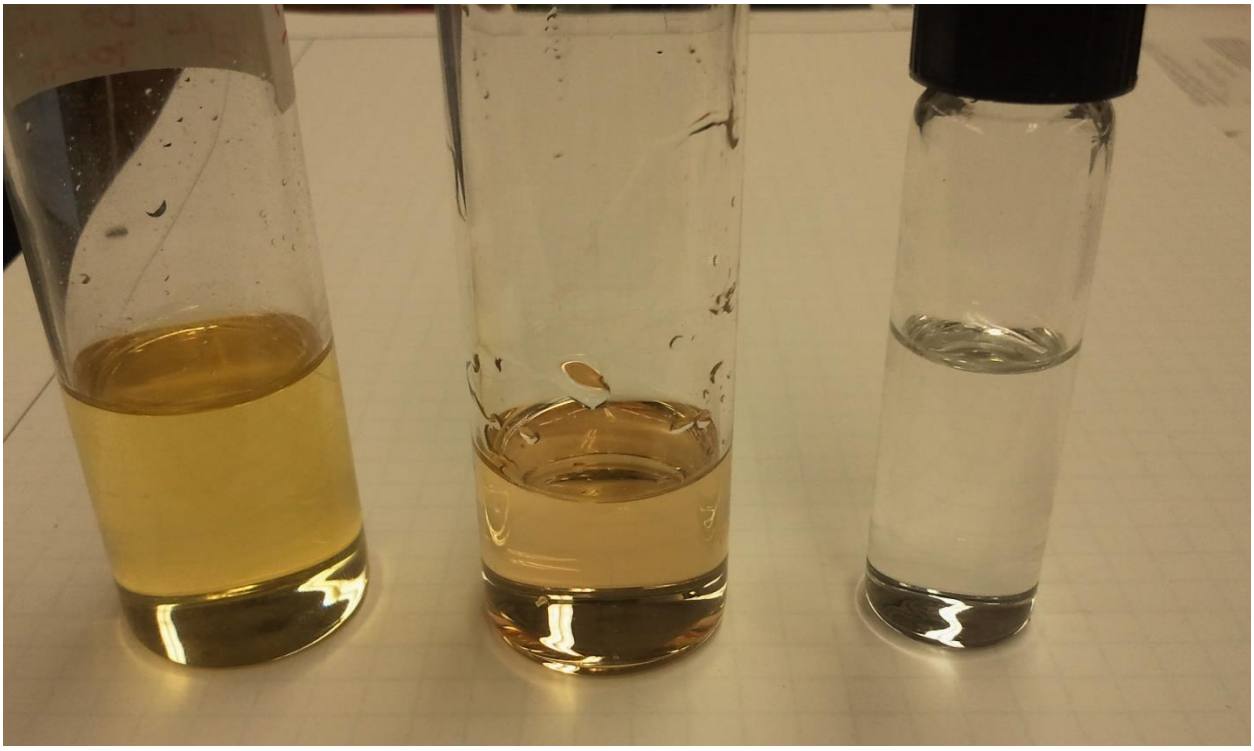

Figure 3.1 – Photograph of three RTILs in different stages of purification. BMIM-Cl post synthesis (left), BMIM-OTf post ion-exchange (centre), purified BMIM-OTf (right).

3.1.3 Handling Requirements

In addition to the potential presence of precursor impurities or side-reaction products, RTILs tend to be hygroscopic. Any level of water or organic solvents dissolved in the RTIL will have a serious effect on the interfacial behaviour and must be eliminated prior to use in any experiment. To ensure the lowest levels of dissolved solvents and water, all RTILs were stored under vacuum or purged with dried high-purity Argon. Prior to use, the BMIM-OTf was heated to 75°C under high vacuum for several hours. The electrochemical cell was also freshly acid washed using a hot 2:1 H_2SO_4:HNO_3 mixture for 30 minutes followed by a rinse step with extensive amounts of Milli-Q water and finally dried in an oven at 120°C for 2 hours. The cell was then assembled and purged with dry Argon. The BMIM-OTf was transferred to the cell using a

purged syringe and needle with a protective plug of Argon drawn into the syringe to maintain dryness of the BMIM-Otf. These procedures ensured a reliable and consistent methodology to maintain a pure and dry BMIM-OTf sample for use in our electrochemical investigations of its capacitive behaviour at a metal interface.

3.2 Electrochemical Methods and Techniques

3.2.1 Cyclic Voltammetry

The first electrochemical technique employed in the analysis of BMIM-OTf was cyclic voltammetry or CV. This method used a typical three electrode configuration – a working electrode, counter electrode, and reference electrode. In this measurement, the potential of the working electrode is cycled between an upper and lower limit along a linear ramp at a fixed rate. The potential of the working electrode is cycled relative to the reference electrode, while the current flowing between the working electrode and the counter electrode is measured. The resulting potential and current data is combined into a plot referred to as a cyclic voltammogram. These plots are useful as they contain potential information regarding both Faradaic (electron transfer reactions) and non-Faradaic (capacitive charging) processes. For fundamental interfacial studies such as the work contained within this thesis, interest lies in the non-Faradaic or double-layer processes. CVs become more informative when a model can be applied to the interface. An R-C circuit model is the simplest model of the double-layer region and is often used to describe this region. The use of models allows for correlations between the current-potential data collected during CV experiments and events or processes at the electrode-solution interface. In this work, this technique is useful for the initial investigation of the response of the RTIL to changing

electrode potentials. Cyclic voltammograms were able to provide an appropriate potential window for the use of BMIM-OTf in further electrochemical measurements.

3.2.2 AC Voltammetry

AC Voltammetry measurements (also known as Differential Capacitance) were used as a secondary probe of the interface once the potential window was determined *via* CV. AC voltammetry is performed by superimposing an AC perturbation over a linear voltage ramp. A typical configuration uses a 25Hz sinusoidal wave with a 5mV (root-mean-square) amplitude. This results in a very slow scan that includes many cycles of the oscillation per unit potential increase. An in-phase (I') and an out-of-phase (I") (relative to the potential perturbation) current is measured using a lock-in amplifier. This data is then used to calculate a differential (serial) capacitance using eq. (3.1).

$$C_d = \frac{I''}{\omega V_{AC}}\left(1 + \left(\frac{I'}{I''}\right)^2\right) \tag{3.1}$$

In deriving eq. 3.1, the interface is modelled as a simple resistor and capacitor series circuit. Taking the total impedance of such an interface, we arrive at eq. 3.2:

$$Z = R + \left(\frac{1}{j\omega C}\right) \tag{3.2}$$

Where R represents the resistance across the interface, ω the angular frequency of the AC perturbation, and C is the differential capacity of the interface. Using Ohm's Law an expression can be obtained for the resulting AC current:

$$I_{AC} = V_{AC}\left[\frac{j\omega C + R\omega^2 C^2}{1 + R^2\omega^2 C^2}\right] \tag{3.3}$$

Which can be separated into a real and complex component, *I'* and *I''*, respectively. Using a lock-in amplifier, these currents can be measured and used to back calculate a differential capacitance using equation (3.1). The DC data is presented in capacity *versus* potential plot, similar to a cyclic voltammogram.

The definition of capacitance plays an important role in understanding capacitance data. If the double layer is modeled as a simplistic parallel plate capacitor, equation (3.4) can be used to give its capacitance

$$C = \frac{A\varepsilon_o\varepsilon_r}{d} \tag{3.4}$$

Where *A* and *d* is the area of and distance between the plates, ε_o and ε_r are the permittivity of free space and relative permittivity, respectively. With the above parameters, *d* is of the greatest consequence, as it describes the distance from the electrode surface to bulk solution conditions and effectively defines the thickness of the double-layer region.

From purely electrochemical theory origins, we can define differential capacity in terms of the surface charge density, σ_m, and the applied potential, *E*, was shown previously in equation (2.2). It is important to note that equation (2.2) is only appropriate in situations where no specific adsorption occurs, as surface charge is described only as a function of applied potential. When ions specifically adsorb, charge density becomes a function of both applied potential and the surface excess, Γ, of the adsorbed ions. Equation (3.5) shows the expression for surface charge density:

$$d\sigma_m = \left(\frac{\partial \sigma_m}{\partial \Gamma}\right)_E d\Gamma + \left(\frac{\partial \sigma_m}{\partial E}\right)_\Gamma dE \tag{3.5}$$

Applying the definition of capacity to equation (3.5), we can now define capacity in terms of both applied potential and surface excess:

$$C = \left(\frac{\partial \sigma_m}{\partial \Gamma}\right)_E \frac{d\Gamma}{dE} + \left(\frac{\partial \sigma_m}{\partial E}\right)_\Gamma \tag{3.6}$$

While AC Voltammetry measurements are useful for determining capacity maxima and minima, they treat the interface as a single capacitive element. This treatment is overly simplified in many cases, and leads to blurring multiple processes together into charging/discharging of a simple capacitor. AC Voltammetry was useful in our initial investigations to provide a basis for further, more advanced capacitance measurements.

3.2.3 Chronocapacity

Chronocapacity is a relatively simple, yet highly useful electrochemical technique that involves measuring the amount of charge passed with respect to time. From a technical standpoint, these measurements are relatively simple. A potentiostat is used to step the potential from some base potential to a potential of interest as quickly as possible while measuring the resulting current over a specified time period. This is known as chronoamperometry. Chronocapacity takes the current versus time transient and applies an integration to obtain the charge versus time transient. A major advantage of the integration of the current is that it provides a means to eliminate noise in the signal. Typical interfacial processes tend to occur on a rapid timescale and require a high sampling rate, which can induce a higher than desirable amount of noise. The idea behind this

technique is to probe surface processes that occur as the interface equilibrates in response to a potential step applied to the electrode. It should be noted that this instantaneous potential step is potentially problematic given that the charging of an electrode or surface, and measuring the response as a function of time is a kinetic process in and of itself, and thus all processes must be considered. The rise time is a measure of a potentiostat's ability to quickly apply a new potential to an electrode. This property is related to the design of the potentiostat and remains relatively constant. One must also consider the time constant of the system under study. The time constant describes how quickly an experimental system can respond to a potential step. Thankfully, in most cases, with modern electrochemical equipment, the rise time is orders of magnitude faster than the electrochemical response and is not a factor in time related measurements. In the studies reported within this thesis, the RTIL interfacial dynamics are much slower than any of the instruments used, so this is not an issue.

3.2.4 Electrochemical Impedance Spectroscopy (EIS)

Electrochemical Impedance Spectroscopy (EIS) is an electrochemical analysis method that studies a system's response to a small magnitude periodic perturbation. It is similar to AC Voltammetry measurements, as in-phase and out-of-phase currents are measured, but EIS employs a variable frequency scheme, while holding the DC potential at a fixed value. The feature benefit of EIS becomes apparent when studying systems with multiple processes occurring simultaneously. The situation becomes even more complex when these multiple simultaneous processes occur on different time scales. By sampling the response of a system over a wide range of frequencies ranging on a scale from a sub-hertz to megahertz, one can begin to isolate different electrochemical processes using EIS. Compared to simple AC Voltammetry measurements which rely on an overly simplified equivalent circuit, which ultimately convolve multiple processes

together into a single capacitive process modeled as the charging and discharging of a simple capacitor.

The methodology behind EIS is relatively simple – a series of AC current and voltage measurements are made across a specific frequency range at a given fixed DC potential. Holding an electrochemical system at a steady potential while imposing a very small periodic perturbation has distinct advantages. With overly slow kinetic systems – such as RTILs – an electrode pre-treatment can be used to establish equilibrium before applying perturbation. By holding the potential steady before making any measurements, we can ensure that the interface has reached equilibrium for a given potential. This minimizes the possibility that interfacial relaxation processes related to the applied potential are still underway at the time of measurement. The end result is a more accurate steady-state measurement. The downside to this process is that a typical experiment will take several hours or more, depending on the number of potentials and the length of the pre-treatment time. These types of experiments require a setup that is both very stable over long time periods, as well as a cell that can maintain the conditions required for a particular system. In the case of RTILs, the cell must maintain an inert and dry atmosphere to prevent RTIL contamination. Additionally, the setup must maintain consistent electrode-RTIL contact. Given that the hanging meniscus configuration is the most popular, any change in the level of RTIL can result in a change in contact area, or worse yet – complete loss of contact between electrode and RTIL.

EIS data is not more complex than other methods, but its handling does involve some mathematical treatment. The application of a small sinusoidal perturbation, V_{AC}, results in a net current measurement, which is passed to the frequency response analyzer, or FRA. The FRA processes the current in an analogous way as a lock-in amplifier (LIA) does and resolves the AC

current into a component that is in-phase with the potential perturbation and a component that is out-of-phase. The benefit of using an FRA is in its speed and wide frequency range. In order to properly cover how the FRA is able to measure the impedance of an interface, some simple AC circuit principles must be understood.

All discussions of electrical circuitry and their response to an input signal at some point break down based on Ohm's law which states that for a purely resistive load the current, *i*, is equal to the potential, *E*, divided by the resistance, *R*:

$$i(t) = \frac{E(t)}{R} \tag{3.7}$$

Since we know that an electrochemical system is not purely resistive and includes capacitive properties, the definition of a capacitance is:

$$C = \frac{q}{E} \tag{3.8}$$

With the definition of current (the rate of flow of charge relative to time), we can use equation 3.8 to derive the relationship between current and potential for a capacitor in equation 3.9:

$$i(t) = C\frac{dE(t)}{dt} \tag{3.9}$$

With equations (3.8) and (3.9) we now have the required relationships. It is important to note that with capacitor at a steady potential, *i.e.* dE/dt = 0, it will behave as an open circuit (after a sufficient capacitor charging time). When a periodic sinusoidal potential, given by equation (3.10) is applied we can see that equation (3.9) becomes equation (3.11) and (3.12) giving the current response of a capacitive load:

$$E(t) = |E|\sin(\omega t) \tag{3.10}$$

$$i(t) = \omega C|E|\cos(\omega t + \varphi) \tag{3.11}$$

$$i(t) = \frac{|E|}{X_C}\cos(\omega t + \varphi) \tag{3.12}$$

where ω is the angular frequency of the signal ($\omega = 2\pi f$), φ is the phase shift between *E(t)* and *i(t)*, and X_C is the capacitive reactance given by $X_C = 1/\omega C$. In the case of a pure capacitance, $\varphi = \pi/2$, *i.e.* the current lags the voltage by 90°. If we consider the voltage and current as phasor quantities on a plane, rotating about a single point or origin, we can define the above equations using complex notation. Components along the ordinate are referred to as imaginary and thus are multiplied by $j = \sqrt{-1}$ while components along the abscissa are termed real. The result is equation (3.13),

$$E(t) = -jX_C \cdot I(t) \tag{3.13}$$

Moving away from pure capacitance or resistance, we must consider a situation that is more akin to electrochemical systems – a resistance and capacitance in series. Noting that the voltage drop across two circuit components in series must be the sum of the voltage drops across each component, we have equation (3.14) which can be expanded using equations (3.7) and (3.13):

$$E = E_R + E_C \tag{3.14}$$

$$E = I(R - jX_C) \tag{3.15}$$

Using equation (3.15) a link now exists between current and potential for an RC circuit. The complex quantity ($R - jX_C$) is referred to as the impedance, *Z*. The impedance is a complex representation of both a real, $Z_{Real} = R$, and an imaginary part, $Z_{Imaginary} = 1/\omega C$. It is important to take note that the impedance is frequency dependent.

EIS measurements are generally performed as a scan from high frequency to low frequency followed by plotting the real vs imaginary components of the complex impedance. The plot begins at high frequency with only the solution resistance, and follows an arc as the frequency decreases as the system is typically under kinetic control with no mass transport effects. As the frequency drops below a certain point (system dependent), mass transport becomes a factor and both the real and imaginary components of impedance increase. Work by Roling, Huber, and Drüschler [39] has proven to be useful in the analysis of impedance spectra. This work involves calculating both real and imaginary components of capacitance using impedance data collected in the traditional format. Complex capacitance data is then presented in a similar plot and is referred to as the complex capacitance plane, or CCP. The major benefit of displaying data in this fashion is the elucidation of multiple processes on different timescales occurring at the interface. Different processes are seen as semi-circles on the complex capacitance plot.

3.2.5 Immersion Method for RTIL PZC Determination

A modified version of the well-known electrode immersion method developed initially by Czajkowski [40] was utilized for determining the potential of zero charge (PZC) of the ionic liquid BMIM-OTf. The basis of this method involves preparing an extremely clean and dry electrode, applying a potential of interest, and bringing the RTIL into contact with the surface as quickly and uniformly as possible. A faradaic charging current is measured as the EDL forms. This is a very fast measurement as the process occurs on the sub-millisecond timescale. The principle behind this technique is relatively simple; immersion of the electrode under an applied potential greater than the PZC will produce a positive current transient, while an applied potential less than the PZC

will produce a negative transient. A simple visual inspection of these transients can narrow the range for the PZC. Using a simple integration of the current-time data, the total charge for the immersion (and EDL formation) can be calculated. Plotting the charge versus applied potential allows one to obtain the PZC.

This technique proved to be very tricky to perform in a reproducible manner. The electrode cleanliness was paramount to collecting meaningful data. A polycrystalline gold electrode was polished to a mirror finish using successively finer diamond paste down to 0.5um followed by rinsing in ultrapure Milli-Q water. Further cleaning was performed in fresh piranha solution (4:1 H_2SO_4 : H_2O_2 mixture) for several minutes. Immediately prior to transferring the electrode to the electrochemical cell, it was flame annealed to a light cherry-red colour in a hydrogen flame 3 times, followed by cooling in a stream of dried Argon. The electrode was then quickly transferred to the electrochemical cell where it was suspended a few millimetres above the dry BMIM-OTf, also under a dry Argon atmosphere. After making connection to the working electrode lead of the potentiostat and beginning data collection, the electrode was slowly lowered to make contact with the RTIL. A HEKA PG590 potentiostat was used in conjunction with a National Instruments data acquisition suite running custom LabVIEW software developed in-house.

The difficulties with this technique lay within making good contact between the electrode and RTIL. In an ideal immersion experiment, the electrode only makes contact with the RTIL on its polished surface with no meniscus wicking up the sides of the electrode increasing the effective contact area. Second, the ideal immersion occurs instantaneously and uniformly across the polished surface. If the contact deviates from these conditions, a variance in the collected current transient will occur. This variance will likely result in measurement of multiple processes rather than isolating the EDL formation.

3.3 Electrochemical Cell Design

3.3.1 The Cell

Electrochemical experiments involving liquids require some form of a containment vessel, most commonly referred to as an electrochemical cell. Not only does the cell need to contain and isolate the liquid from the surrounding environment, but it also must provide a solid way to mount and house all electrodes, gas inlets and outlets and any other various ports as required by the specific experiment. In the case of working with RTILs that are not easy to synthesize and purify economically in large amounts, an electrochemical cell was designed and built over several iterations. The first priority with this new cell design was to minimize the volume of RTIL required for each experiment. The design consisted of a narrow borosilicate glass tube with one end sealed flat and a male ground glass joint on the other. The tube sits vertically with the sealed end down creating a tall and narrow cell. A reference electrode port was added at the bottom of the cell. A cap was also made that had one central port for the working electrode and its holder. In addition, four ports arranged around the centre were added to allow entry for the counter electrode, gas in and out, as well as one to fill the cell via a syringe. Initially, all major joints were assembled using the BMIM-OTf as a sealant. This practice was abandoned due to fears of the sealant RTIL pulling air or moisture from the environment. All joints were subsequently sealed using a high vacuum grease, or Teflon plugs in combination with paraffin film. Additionally, a constant positive pressure of dry high-purity Argon ensured a dry and contaminant free cell once assembled.

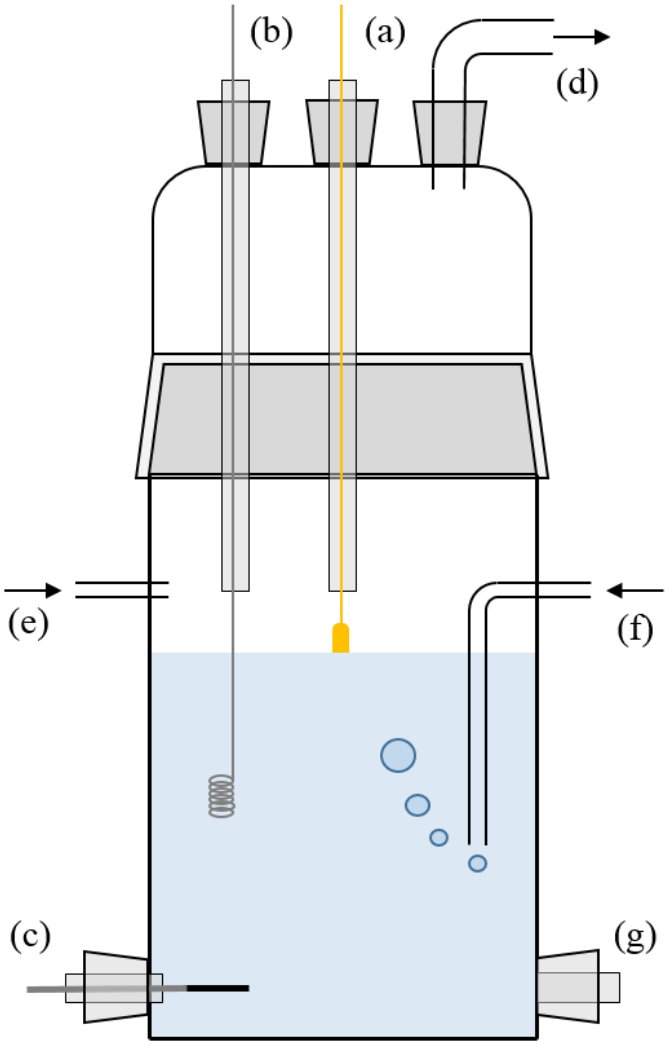

Figure 3.2 – Electrochemical Cell Schematic with labelled parts: (a) Working electrode in hanging meniscus configuration, (b) Platinum wire counter electrode, (c) Reference electrode port, (d) purge-gas out port, (e) purge-gas in port, (f) down-bubble purge gas port, (g) RTIL level modulation port for syringe.

3.3.2 Salt Bridge

Initially, due to the first reference electrode used, a standard electrochemical salt bridge was employed to set up the electrochemical cell. The so-called salt bridge is typically used on standard aqueous-based electrochemical cell setups to isolate the reference cell compartment from

the rest of the cell while ensuring ionic conductivity between the reference electrode and the working electrode. It uses a holder with a ground glass stopcock lubricated by the electrolyte solution to maintain ionic conductivity but limit mass transfer to minimize any contamination. This salt bridge was utilized in the same fashion for the RTIL setup, the petcock was lubricated with RTIL during assembly.

As this project moved forward, evidence suggested that the salt bridge not be necessary with a different type of reference electrode. This progression is discussed in the next section. Due to the change in the reference electrode, the salt bridge was removed and the reference electrode was directly immersed in the main body of the cell with no contamination or stability issues.

3.3.3 Reference Electrode Progression

The role of the reference electrode is very important to electrochemical research – a stable potential to which all other potentials are referenced is vital for repeatability and consistency across multiple trials and different types of experiments. The keys to an excellent reference electrode system is stability – during both use and storage, as well as ease of handling and assembly. For the first few experiments, we chose to follow the method outlined by Huber and Roling [41] and built a Ag/Ag^{+} using existing glassware from previous electrochemical reference electrodes. The electrode body was a borosilicate glass tube fitted with a medium-porosity fritted glass disk at one end and a female ground glass joint at the other. A silver wire (1mm, Sigma Aldrich) was then sealed into a male ground glass joint to fit into the holder. The reference cell was then filled with solution of silver triflate (10mM) dissolved into the BMIM-OTf RTIL. This configuration produced a stable reference potential over the timeframe of one set of experiments, generally 24-

hours. However, we encountered some difficulties with the Ag^+ ions photoreducing and precipitating out of solution. This problem was noticed visually as a soiling of the fritted glass bottom of the cell holder. This effect was minimized by storing the reference electrode in darkness. The issue with Ag^+ precipitation is a drift in the reference electrode's potential, which in turn shifts any applied potential and continuity across multiple experiments is lost unless the drift can be quantified.

A simpler solution was sought to minimize the instability of the Ag/Ag^+ in BMIM-OTf reference described above. Ideally, for this type of experiment, we would prefer a reference electrode with a minimal number of connections or joints to minimize potential leaks or sources of contamination. With contamination in mind, it would also be ideal to have only pure RTIL used in the reference electrode. In attempt to satisfy these ideal requirements, a simple reference electrode was conceived as an Ag wire coated in AgCl directly immersed in the BMIM-OTf without the salt-bridge assembly. This configuration proved to be highly successful over many experiments. There was no evidence of deterioration or drift with this version of the reference electrode. The reference potential from this electrode was stable and verified prior to each experiment via cyclic voltammetry.

3.3.4 Impedance Shunt Development

The first version of the reference electrode used a reference cell and holder that included a salt-bridge. This design was taken from existing electrochemical cells designed for aqueous systems. With a standard ground glass petcock lubricated with RTIL, the so-called salt-bridge and fritted glass electrode holder introduced a stray impedance between the reference electrode and the

counter electrode. This became evident during EIS studies as a stray impedance appeared as artifacts during the high frequency portion of the measurement. Fafilek [42] showed that a simple shunt capacitor (10nF) wired between the reference and counter electrodes can be used to circumvent the stray impedance.

When the reference electrode migrated out of a holder and directly into the RTIL in the main body of the cell, the need for this impedance shunt was eliminated. Ultimately, this reduced the complexity of the cell and its setup, as well as reduced the number of joints that were potential contamination sites, or leaks.

3.3.4 Immersion Cell Modification

Conducting the immersion experiments proved to be the most technically challenging portion of this project. The challenges associated with this style of experiment were solely related to achieving consistent and uniform fast contact between the RTIL and the electrode surface. The first methodology employed used the identical setup as the impedance experiments. With the clean electrode in the cell and the appropriate potential applied, the electrode is manually pushed downwards to make contact with the RTIL. This method was problematic – it was difficult to minimize RTIL "creep" up the sides of the electrode. When pushing a relatively solid mounted electrode downwards, it was difficult to achieve the same depth on subsequent runs resulting in discrepancies in the resulting current transients.

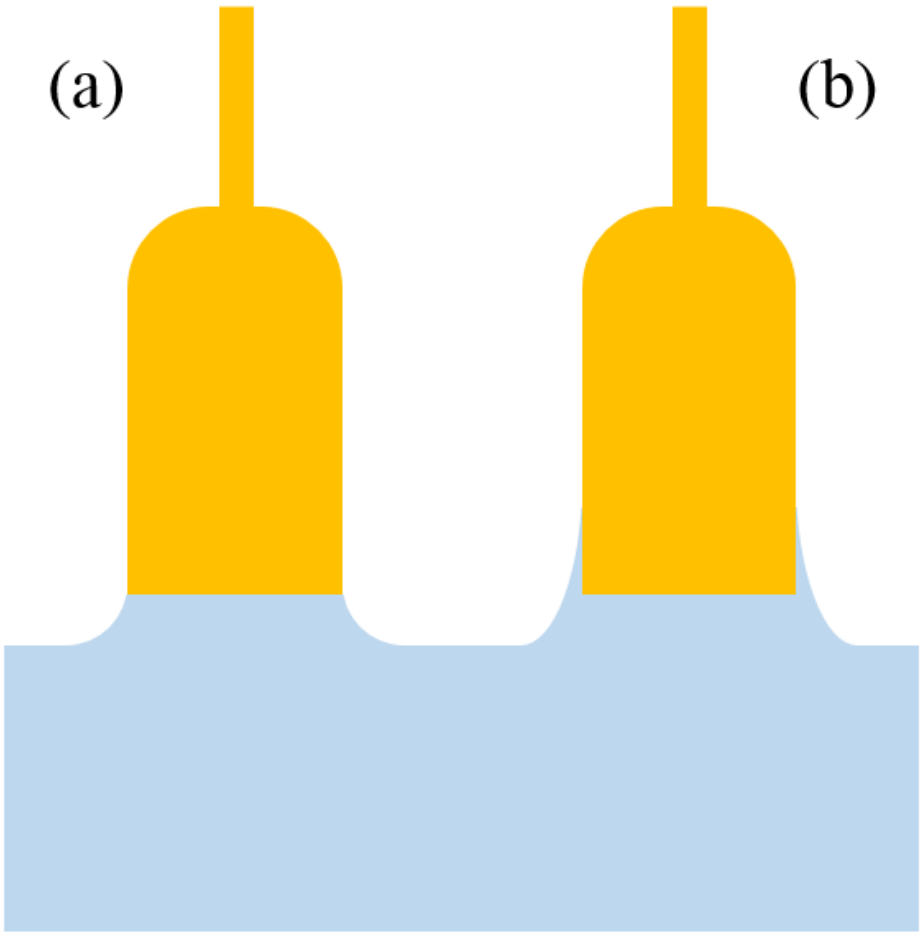

Figure 3.3 – Immersion experiment meniscus configuration – a proper meniscus (a); evident sidewall creep and over-immersion (b).

To counter this issue, we approached the problem from the other direction. Instead of attempting to move the electrode toward the RTIL, we modified the cell to allow us to move the RTIL closer to the solid mounted electrode. The main cell body was modified by adding a second joint at the bottom, identical to the port for the reference electrode. In this port a glass syringe was fit, allowing the level of the RTIL in the cell to be modulated by moving the plunger of the syringe in

and out. Using this methodology, we were able to increase the level of repeatability to the immersion experiments and achieve a consistent meniscus between the RTIL and polycrystalline Au electrode surface with minimal sidewall creep.

CHAPTER 4

ELECTROCHEMISTRY COMMUNICATIONS PAPER & RELATED WORK

This chapter outlines the initial electrochemical investigations of the high purity BMIM-OTf RTIL that was published in *Electrochemistry Communications*, **2010**, *12*, 1340. The following is not a copy of the paper, but rather a rewritten and expanded look at the research that the aforementioned paper was based upon.

4.1 Introduction

As mentioned previously in this thesis, there exists a knowledge gap between theory and experiment regarding the interfacial behaviour and structure of the RTIL | metal interface. The shortcomings of current models that are based upon the classical dilute aqueous electrolyte systems have been well documented in a recent critical review by Alexei Kornyshev [43]. Work by Oldham [44] has shown that by modifying the standard Guoy-Chapman-Stern model, the general capacitance behaviour of the interface can be modelled. Another approach to modelling the interface was undertaken by Kornyshev involving molecular dynamics simulations that shed light on layering effects in the double-layer region [45-47]. At the PZC, where a capacitive minimum is expected for a dilute electrolyte, these modelling attempts predict a capacitive maximum for an incompressible ionic liquid. It is important to note that if the ion size difference is significant, the RTIL can be considered to be compressible to a certain degree, which futher results in a double-humped or "camel" shaped capacitance-potential plot.

Theoretical approaches provide a strong insight into the structure and general behaviour of the interface, but experimental results are far more complicated than theory predicts. The literature is filled with investigations of the interfacial capacitance behaviour of many different RTILs on many different electrode materials ranging from poly-crystalline [48-51] and single-crystalline metals [52-54], Mercury [48, 55-57], as well as conductive carbon electrodes [48-50, 57, 58]. Reviewing the wide array of reported capacitance-potential (C-E) curves, a large variance with three general shapes evident: parabolic, bell-shaped, and camel-shaped. With the plethora of possible influencing factors considered, the common denominator between all of these C-E curves is the type of electrolyte. This leads to our focus on the handling and purity of an ionic liquid in electrochemical experiments. Inherently, these materials tend to be difficult to handle while maintaining a high level of purity. The aforementioned papers fail to take a systematic approach to ensure the highest level of ionic liquid purity.

To further the discrepancies across the literature, many studies utilize electrochemical techniques that use single frequency measurements. The problem with this approach is that these measurements assume an ideally polarized interface that results in a series capacitance, C_S, and not necessarily a pure capacitance for the double-layer region, C_{DL}. With this in mind, adsorption kinetics have been shown to significantly influence the series capacitance [52, 59], and as such, care must be taken to isolate C_{DL} from C_S. A second point of note regarding previous studies relates to the viscosity and relatively low ion mobility of RTILs. Physical properties like high viscosity and low ion mobility, as ionic liquids tend to have [60], induce relatively long equilibration timeframes in response to changes in applied electrode potential. Ultimately, this slow response works itself out as interfacial relaxation that is much slower than the analytical technique's electrical perturbation.

The variance seen across the literature is likely the compound product of many of the issues outlined above. The work contained within this chapter covers our attempt to address and rectify some of these issues in pursuit of the complete picture of the RTIL | metal electrochemical interface. This work began upon arriving at an acceptably high purity BMIM-OTF product, whereupon we began to characterize the RTIL behaviour with basic electrochemical methods.

4.2 Initial Investigations using Cyclic Voltammetry

Initital investigations of RTIL electrochemistry began with cyclic voltammetry to determine the current response and applicable potential range for further experiments. We knew that the range of potentials that these ultra-pure RTILs was wide, but did not expect it to be as wide as the 3.5V we eventually encountered. We found that we were able to apply potentials ranging from +1.0V to -2.5V with very low current until the extreme potentials at either end of the range were reached. This method was initially used as a way to identify the potential limitations for further experiments. The aim was to explore the useable and safe region for applied electrode potentials. Avoiding sharp exponential changes in current as the potential was increased was important to avoid triggering any non-Faradaic processes that ultimately break down the RTIL rendering it impure. We found that prolonged time at these potentials resulted in irreversible changes in the CV. It is likely that potentials in this range are driving reactions that breakdown the RTIL and/or poisoning of the electrode surface. Aside from the end-regions, the CV's appeared to be nearly featureless and rather flat in the middle (or capacitive region), as seen in Figure 4.1.

Our initial scan rate was 50 mV/s – which, for CV measurements, is not overly fast. However, we did suspect that due to the higher viscosity and lower ion mobility of RTILs that equilibrium was

a slow and drawn out process in the face of changing electrode potentials. A closer look at CV data using more moderate potential limits and a slower scan rate (20 mV/s), several features were now visible. It was now evident that in scanning the electrode potential out to the limits of the RTIL tended to hide some of the features in the flat region. Figure 4.2 shows a voltammogram with a single peak appearing in the anodic scan, and a double-humped feature in the cathodic scan.

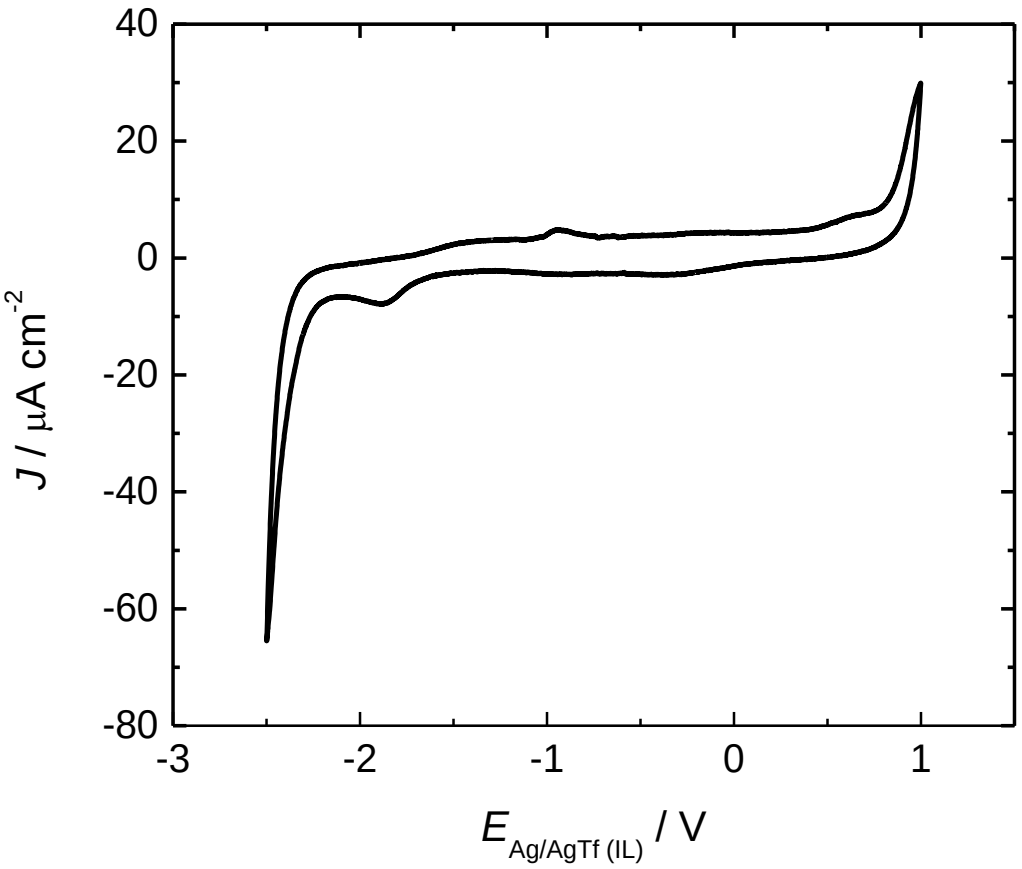

Figure 4.1 – Cyclic Voltammogram (50mV/s) of BMIM-OTf on Polycrystalline Au

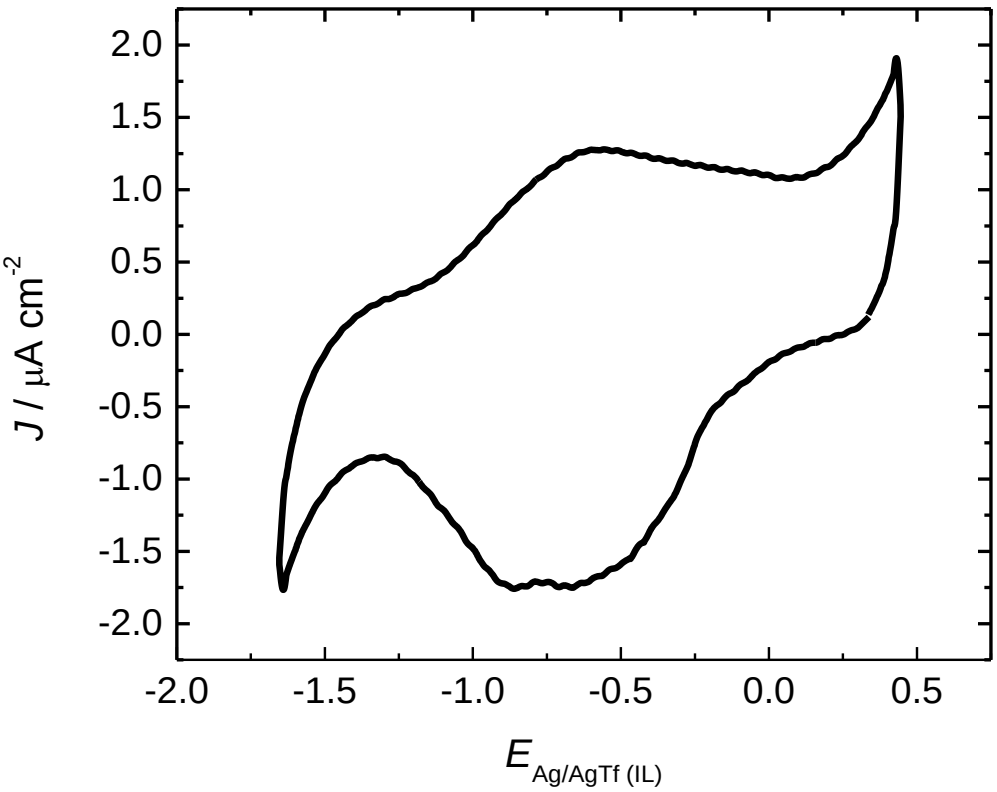

Figure 4.2 – Cyclic Voltammogram (20 mV/S) of BMIM-OTf on Polycrystalline Au

Comparison to the literature showed that our results were very similar to those of Gnahm *et al.* for a Au(100) | $BMIMPF_6$ interface ($BMIMPF_6$ is the hexafluorophosphate anion version of our ionic liquid, BMIM-OTF) [53], as well as $EMIMBF_4$ (1-ethyl-3-methylimidazolium tetrafluoroborate) on polycrystalline gold [61]. Explaining these features is difficult without further information, but due to the low magnitude of the measured current, we concluded that these currents were in fact Faradaic charging currents and their contributions were limited to structural

rearrangement of the double layer region. The next logical step in this progression was to try some AC Voltammetry measurements to further probe the interface.

4.3 AC Voltammetry and Hysteresis Effects

AC Voltammetry, as explained in the previous chapter of this thesis, is a method used in standard electrochemical analyses, so it was a simple and logical next-step for this project. We were able to produce interfacial capacity curves using AC voltammetry – a 5mV/s linear potential ramp with a superimposed 5mV (RMS) sinusoidal perturbation at a frequency of 25 Hz. The use of a lock-in amplifier allows the measurement of both an in-phase current, I', and out-of-phase current, I''. These two currents, when combined with assuming the interface is ideally polarized and applying a simple series R-C circuit results in Eq (4.3.1)

$$C = \frac{I''}{\omega V_{AC}}\left[1 + \left(\frac{I'}{I''}\right)^2\right] \tag{4.3.1}$$

where V_{AC} and $\omega = 2\pi f$ correspond to the root-mean-square amplitude and angular frequency of the sinusoidal perturbation, respectively. Using the collected current data in conjunction with equation 4.3.1 we can calculate the capacity and produce a capacity-potential plot. Figure 4.3 shows the AC voltammetry result for BMIM-OTf. In this experiment, the scan began at 0.0V and proceeded towards the upper limit of 0.4V followed by a scan to -1.65V and back to 0.4V.

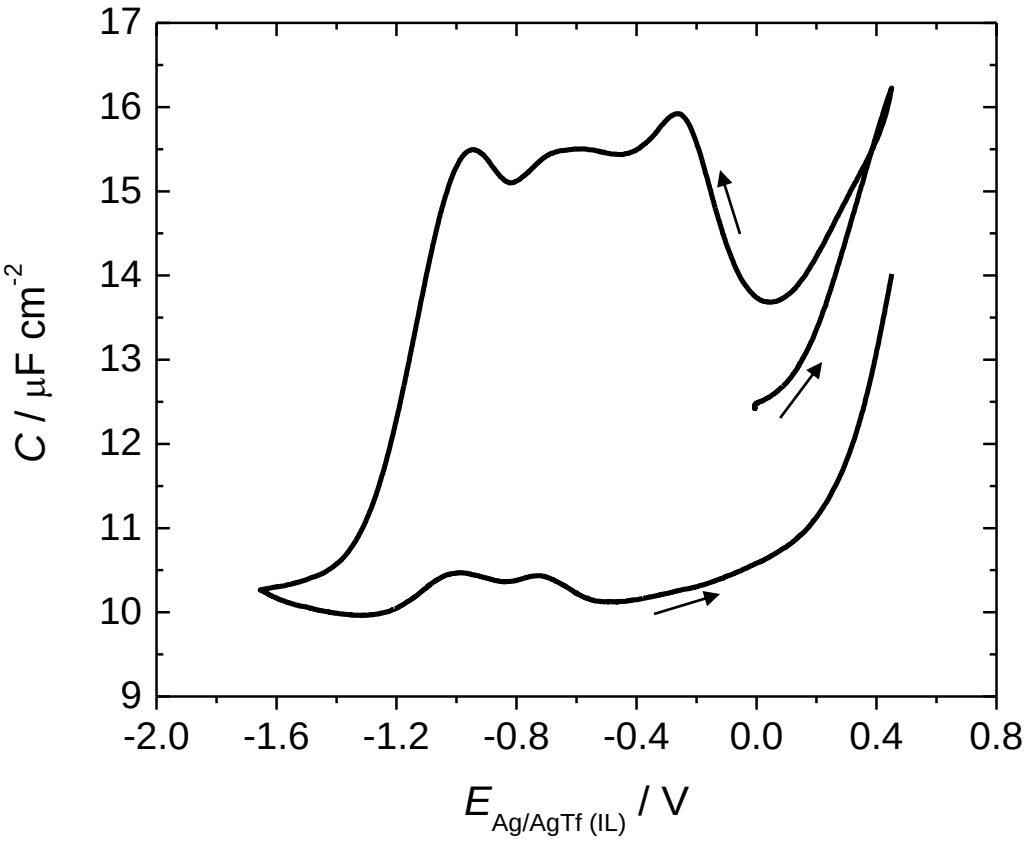

Figure 4.3 – AC Voltammogram of BMIM-OTf on polycrystalline gold

Immediately upon visual inspection of the AC voltammogram, a large hysteresis is visible between the forward and reverse scans. This is to say that when moving the potential in the negative direction, the interfacial capacitance is greater than when moving in the opposite direction. This indicates that there is a different energy cost to changing the surface potential from positive of the PZC to negative of it. The reasons behind this likely lie within how a cation dominated double layer packs and arranges itself compared to an anion dominated double layer region. In addition, the different scan directions reveal a different set of features. The positive going scan shows two distinct features, while the negative going scan clearly exhibits three. The

possibility exists that where the experiment begins is going to dictate what features and/or hysteresis effects are seen. To further the situation, the conclusion can be drawn that the interface exists in two very different states (at either end of the potential range) that have very different levels of stability. Immediately, the cation/anion size asymmetry is likely playing a key role in the occurrence of these hysteresis effects. To uncover the nature of the hysteresis effects on the interfacial capacitance we employed chronocapacity to gather more data on how the interface responds to changing potentials.

4.4 Chronocapacity – Slow Interfacial Relaxation

Chronocapacity was next employed to probe this interface. These experiments involved maintaining a DC potential of -1.2V (below capacitive peaks in the AC Voltammetry experiments) for 10 minutes followed by a rapid step to a more positive potential, noted as E_{step}. The potentials of E_{step} were varied from -1.0V to +0.25V to encompass the features uncovered in the AC Voltammetry experiments. When E_{step} was varied between -1.0V and -0.5V, the capacity transient shows a sharp initial spike followed by a rapid decay to a constant value in a matter of a few minutes. However, when E_{step} rose above -0.5V the transient shape exhibited a vastly different shape. Following the sharp initial spike, the capacity dropped to a minimum then began to slowly rise and reach a near constant value. This process was much slower than that of potentials below -0.5V – nearing ten minutes to reach the near constant value. Figure 4.4 shows the overlaid transients for comparison.

Based upon this data, it appears that a different process takes place on either side of -0.5V. Moreover, the interfacial capacity has been shown to be varying within this ten minute window due to the extremely long relaxation time. Analysis of these capacity transients and their features

indicates a similarity to those expected for nucleation and growth kinetic processes. It follows that the physical interpretation of the interface at -1.2V is a predominantly cation layer on the surface with the anion populations increasing as distance from the electrode surface increases. This would match with Kornyshev's theoretical predictions, as outlined previously. Upon stepping the potential to a more positive value, the surface becomes highly disrupted. The capacity spike is likely due to a compression effect as the interface responds to the rapid change in applied potential. This is followed by a capacity minimum which can be explained as an interface in a state of total disarray as a slow rearrangement takes place. This indicates that the mobility of the ions is low and takes significant time to reach equilibrium and is confirmed by the slow rise of the interfacial capacitance.

Although it is not a concrete conclusion, it is apparent from a visual inspection of the capacity transient shape that as the potential of E_{step} increases, the time to equilibrium decreases. The same can be said for potentials much closer to the hold potential of -1.2V. A group of potentials between the two extremes seems to take considerably longer to reach an equilibrium state. The reason for this is suspected to be that these potentials are closer to the PZC of this interface. As the difference between applied potential and the PZC decreases, there is less of a driving force to modify the RTIL structure within the double layer region. Conceptually, it is simple to consider the point at which E_{step} crosses the PZC and the surface (from the perspective of the RTIL) changes from a negative to positive charge. Since these experiments begin with a surface condition far below the proposed (and plausible) PZC, we can assume a negatively charged surface exists with a cation dominated double-layer region.

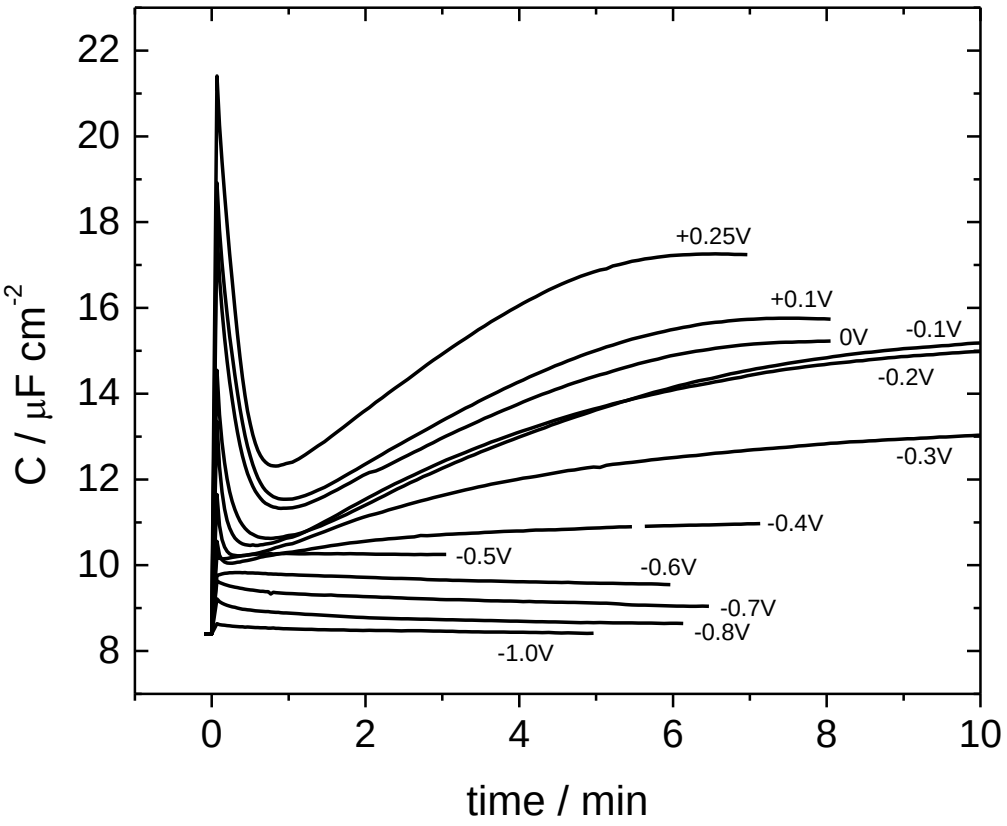

Figure 4.4 – Capacitance (time) transients for BMIM-OTf captured as potential is stepped from -1.2V to the specified potential

With this in mind, it would be expected to see a change in the capacity behaviour once the stepped potential crosses to the positive side of the PZC, rendering the surface positively charged. The data in Figure 4.4 shows a marked change in the capacity transient shape as the stepped potential reaches -0.3V.

Regardless of the shapes of these transients, the importance of this data lies within uncovering the slow response of the RTIL | metal interface. Ultimately, this data leads us to urge caution when interpreting capacitance data for these types of interfaces. Considering that at this

point in time the literature was full of RTIL capacitance results, it was obvious that this result was of high value to the interpretation of such data. To avoid any potential problems with long equilibration times we opted to further probe the interface using EIS at discrete DC potentials. The initial EIS results were also contained within this *Electrochemistry Communications* paper, but will be covered in the next chapter alongside further EIS studies that have not been published.

CHAPTER 5

EIS DATA AND IMMERSION EXPERIMENT RESULTS

This chapter of this thesis covers the second half of published work from *Electrochemistry Communications 12*, **2010**, 1340, as well as newer EIS data that has not yet been published. It will also include data from a set of immersion experiments conducted following the EIS data and will conclude the work contained within this thesis.

5.1 EIS Results – Confirmation of Multiple Processes

Upon the realization that this particular electrochemical interface was perilously slow to reach equilibrium, Electrochemical Impedance Spectroscopy (EIS) was chosen for several reasons. First, EIS allows for separate measurements or experiments at discreet DC potentials. Probing the surface in the frequency domain after holding the DC potential steady for 10 minutes gives a close look at the behaviour of an interface at equilibrium. Second, EIS has the distinct advantage over AC Voltammetry measurements simply because it allows us to perturb the interface at a steady DC potential and varying frequency, whereas DC sweeps the dc potential at a fixed frequency. The upshot is that while DC measurements provide only a series capacitance, EIS can be used to separate out different capacitive components (or processes) across an interface.

The first EIS experiments carried out with BMIM-OTf on polycrystalline gold followed a similar regime to that of the DC experiments. We began with a series of positive going potentials

immediately followed by the same series in the reverse direction. The collected EIS data was used to compute a series capacitance, C_s, given by

$$C_s = \frac{1}{2\pi f Z''} \tag{5.1.1}$$

Where f is the perturbation frequency (in Hz) and Z'' is the measured complex impedance in Ohms (Ω). Figure 5.1 shows a plot of the computed C_s vs E for this series of experiments taken at f = 25Hz.

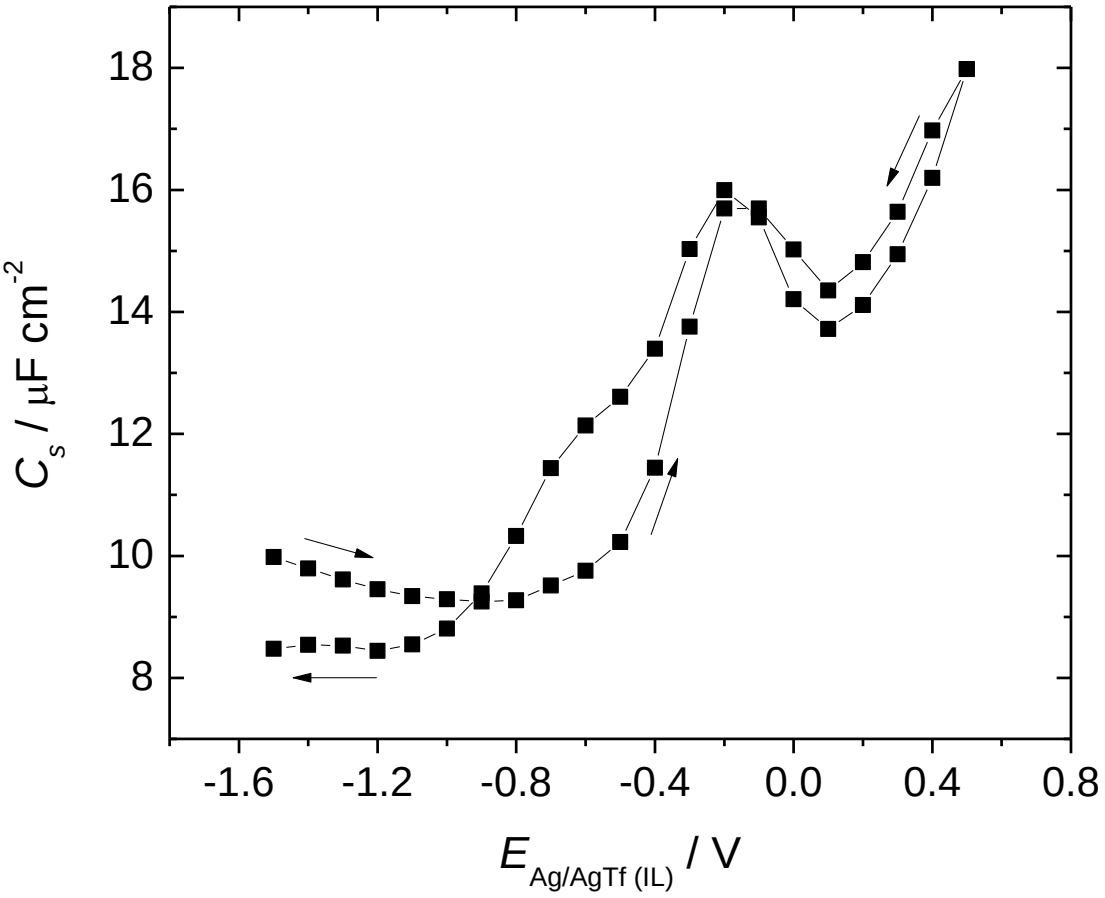

Figure 5.1 – Series Capacitance data collected using EIS (f = 25Hz) for BMIM-OTf on polycrystalline gold

This data clearly shows a hysteresis between the forward and reverse scans, however, it is not nearly as dramatic as the hysteresis observed in the DC experiments. The shape of the single frequency series capacitance anodic and cathodic scans is of particular interest. The anodic scan exhibits a bell-shaped curve while the cathodic series shows somewhat of a camel-shaped double hump feature. Keeping the single frequency aspect of Figure 5.1 in mind, a frequency dependence analysis of C_s for the positive going series is shown in Figure 5.2.

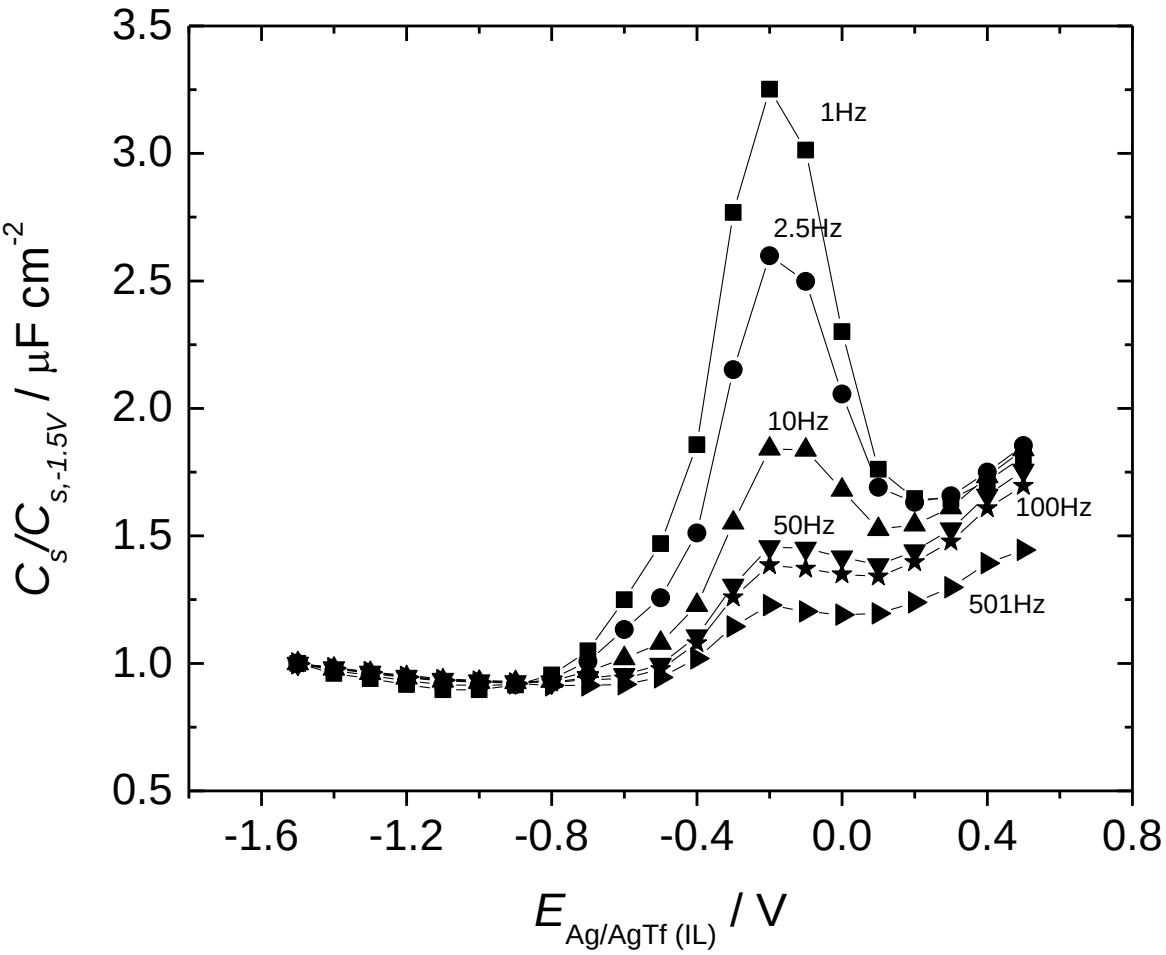

Figure 5.2 – Frequency dependence analysis of C_s EIS data. All values have been normalized to their corresponding C_s value at -1.5V.

Each value used to construct the plot in Figure 5.2 was normalized against its C_s value at -1.5V. This normalization was simply used to clarify the data and show a distinct frequency dispersion. The implications of this dispersion relate back to the initial analysis of this interface with an equivalent circuit, where a simple R-C circuit as assumed to be adequate. Figure 5.2 directly illustrates why a simple RC circuit is not sufficient for modelling the RTIL | metal interface. A single series capacitance is not able to properly account for all capacitive processes occurring at the interface.

The next step in this project was further analysis of the collected data. Instead of applying a simple RC circuit model, we attempted to use a mathematical fitting method employing an equivalent circuit (EC) that involved more than once capacitive element. The EC used for this analysis was relatively simple and combined two RC circuits. The bottom inset in Figure 5.3 illustrates this EC. A capacitive branch was added in parallel to the double layer capacitance to model the kinetics of ion adsorption. The fitting to this data was performed with ZPlot/ZView software (Scribner Associates). Figure 5.3 shows a sample of the impedance data with fitted curves. The scale of this plot may seem to have been selected poorly, but a 1:1 ratio of the ordinate and abscissa is common for this type of plot. The reason behind this is to give a visual relation to the measured real and complex impedances. The top inset of Figure 5.3 shows the same data in a Bode representation.

Fitting this EC to the impedance data proved to be difficult if both capacitive elements were modelled as pure capacitors. At potentials below +0.1V, the adsorption branch of the EC is dominant, but at more positive potentials the R_{ads} value became so large that at even the lowest frequency (0.1Hz) all current was passing through the double-layer arm of the EC. This bypass

resulted in very poor fitting. Moving both elements to Constant Phase Elements (CPE's) vastly improved the results of the fitting.

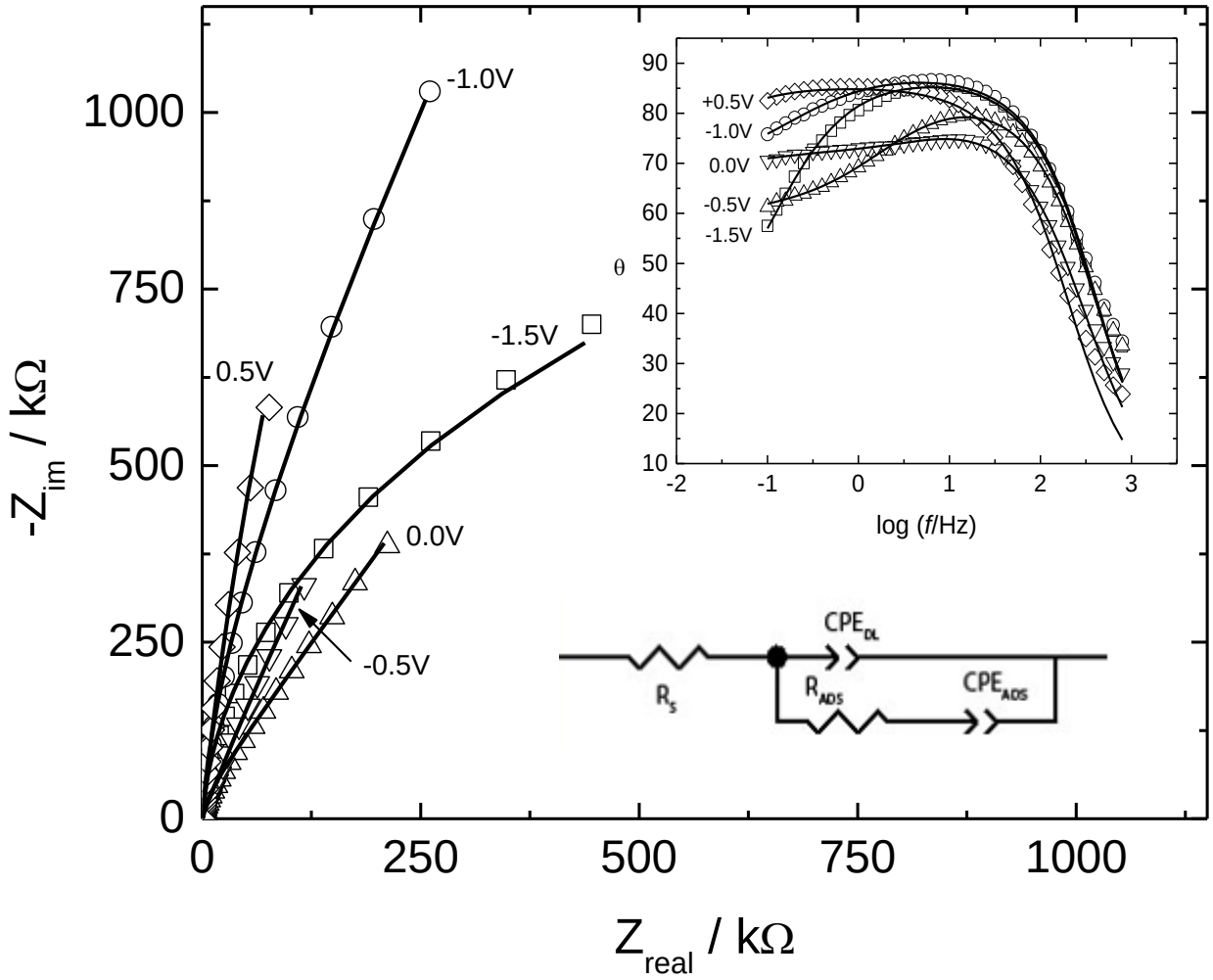

Figure 5.3 – Raw EIS data and Nyquist representation (inset) for BMIM-OTf on polycrystalline gold with fitting to the equivalent circuit with and adsorption component.

The CPE itself has a complicated and ill-defined physical significance, but its purpose is to allow for deviations from a perfect capacitance. These deviations are most commonly attributed to the level of non-homogeneity of the surface. The impedance of a CPE is given by equation 5.1.2:

$$Z_{CPE} = \frac{1}{Q(j\omega)^{\alpha}} \tag{5.1.2}$$

where Q is the CPE coefficient, ω is the angular frequency ($\omega = 2\pi f$), and α is the CPE exponent. The important parameter to understand is α, for when $\alpha = 1$ the CPE behaves as a pure capacitor and Q has units of capacitance, i.e., F/cm^2. When $\alpha \neq 1$, the units of Q become s$^{\alpha}$/Ωcm^2 a perfect capacitive element is no longer modeled. It is of particular interest to note that there are specific values of α that are of interest. At $\alpha = 0$, the CPE behaves as a resistor, and at $\alpha = 0.5$ it becomes a Warburg element [62]. The Warburg element models diffusion of ions to and from the electrode. The presence of fitting parameters nearing $\alpha = 0.5$ are indicative of diffusion limited kinetics of adsorption processes. Figure 5.4 shows a combination plot of the fitted parameters, Q_{ads} and α_{ads}, for the parallel adsorption branch of the EC.

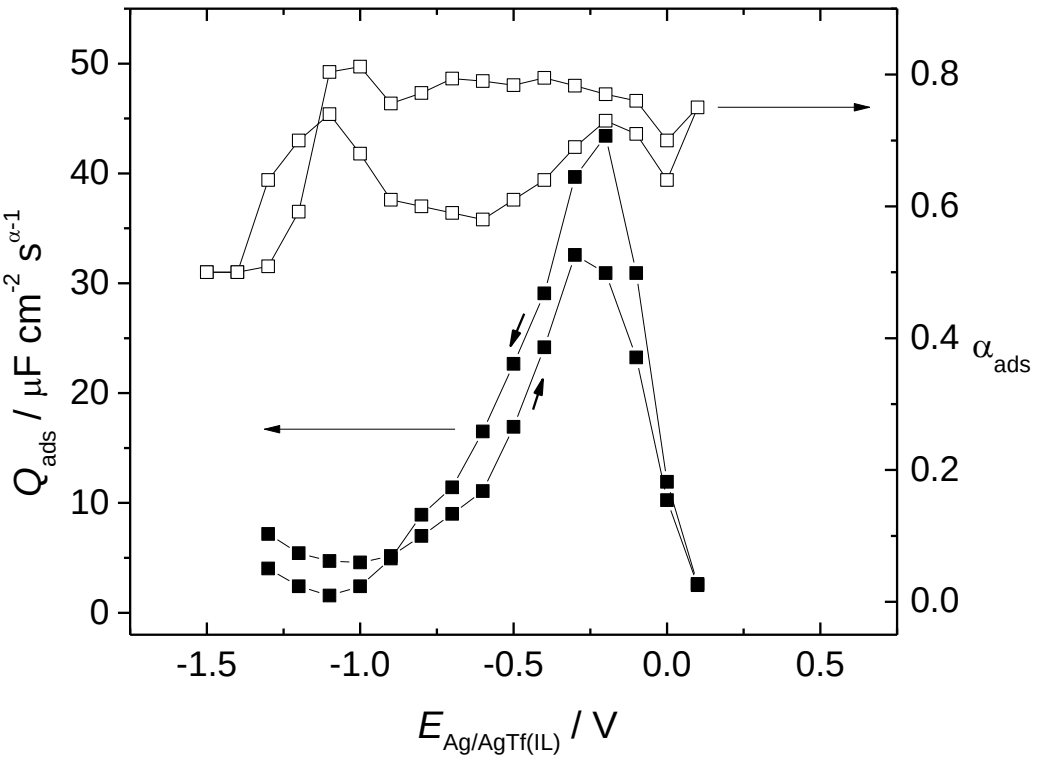

Figure 5.4 – CPE fitted parameters for the adsorption leg of the equivalent circuit.

Given that this data shows a large variance in α_{ads} values, drawing strong conclusions on Q_{ads} is relatively difficult. However, the peak in Q_{ads} at E = -0.2V is a strong sign that the adsorption pseudocapacitance makes up a large component of the overall or serial capacitance of the interface. A similar peak was reported by Gnahm *et al*, where they concluded that this feature was a result of a redistribution of charge in the innermost layer [63]. Such a reorganization of the interface would suggest that the PZC lies in and around this peak at E = -0.2V. This conclusion would be in agreement with the kinetic effects shown by the chronocapacity experiments outlined in Chapter 4.4 (See Figure 4.4). These capacity transients show a definite shape change as the potential moves past -0.5V towards the Q_{ads} peak at approximately -0.2V where the proposed PZC lies.

Analysis of the fitted data for the double layer capacitance CPE appears in Figure 5.5 and immediately one can see the values for α_{DL} remain within a much narrower range very near α = 1. With α_{DL} values as shown in Figure 5.5, we can comfortably conclude that Q_{DL} values accurately correspond to C_{DL}, the double layer capacity. Accounting for the deviations from a true (or perfect) capacitance can be achieved by considering the heterogeneities of the polycrystalline gold surface [64]. Such a surface exhibits many different morphologies resulting in differing capacities for each different region.

The shape of the capacitance-potential plot in Figure 5.5 is of interesting importance. As before in the serial capacitance experiments, hysteresis is evident – but moreover, two distinct shapes are produced for the cathodic and anodic series.

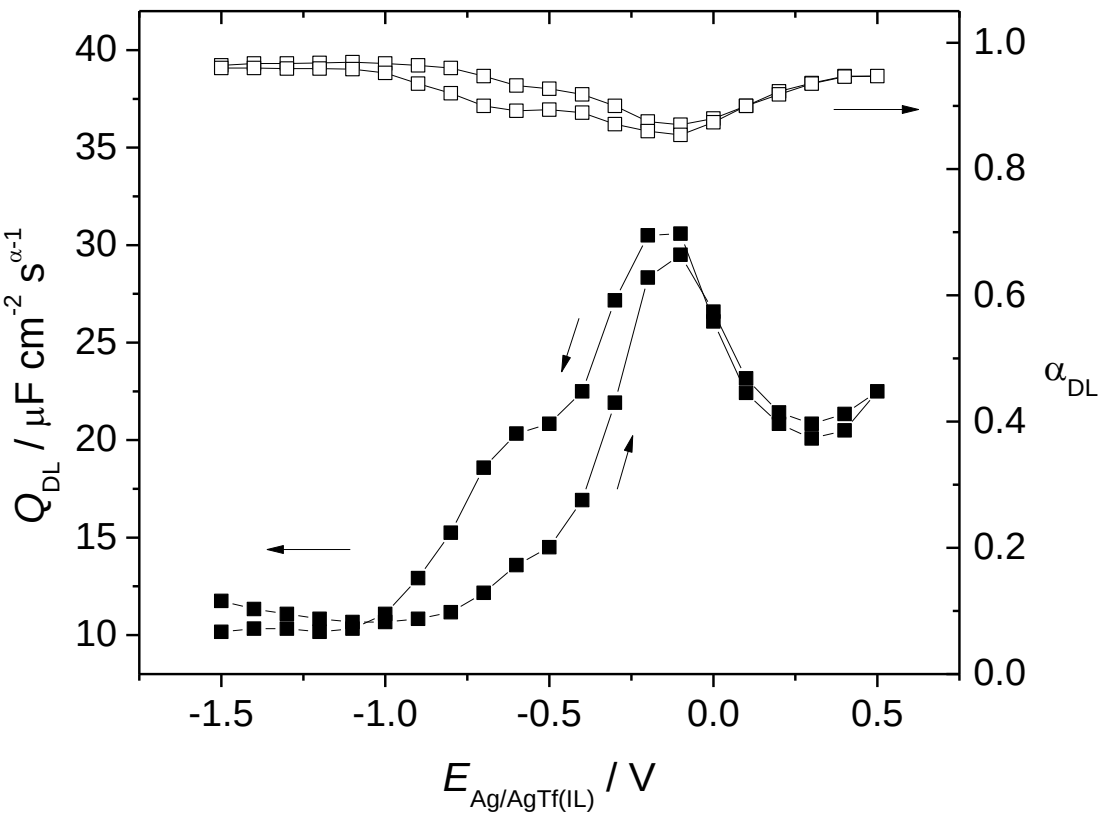

Figure 5.5 – CPE fitted parameters for the double layer component of the interfacial capacity.

The positive going sweep shows a bell-shaped curve, while the negative going progression shows the characteristic camel-shaped, or double-hump feature. In comparison with Kornyshev's MFT-based treatment, the positive going steps agree completely [65]. The capacitance at negative polarizations is significantly less than that of positive polarizations. This can be rationalized by the ion size asymmetry of approximately 2:1 by volume between the BMIM cation and triflate anion of the RTIL [66].

In summary of this portion of the EIS studies of the BMIM-OTf | polycrystalline Au interface, it has been shown that this system exhibits hysteresis effects that are directionally dependent upon the potential and ultimately the surface charge relative to the PZC. Additionally,

the relaxation times for this system have been shown to be extremely slow and must be taken into consideration during critical analysis of data. Due to the large number of varied results described in the literature, caution must be exercised when using any of this data. Furthermore, this work has shown that using a simple RC circuit to model this complex interface is, in fact, too simple. An RC circuit plainly fails to account for the true double layer capacitance in conjunction with complicated adsorption kinetic events also occurring at the interface. Multiple capacitive processes demand equivalent circuit models that contain multiple capacitive elements in order to effectively model the processes at the interface.

Addressing the source of the hysteresis between forward and reverse scans is not straight forward in any sense. We initially proposed that the source of the hysteresis is a result of metastable states of the ion layer nearest the electrode surface. The idea is that this layer is bound tighter than expected as a result of both electrostatic interactions between the surface, neighbouring ions, as well as the compressive force of subsequent layers that extend out away from the electrode surface. These forces then combine to create an energy barrier that needs to be overcome before the interfacial configuration and ultimately its capacitance changes – giving the hysteresis effects shown in this thesis. Several other potential contributions have been posited including, but not limited to: contaminants from the synthesis, water contamination, and/or surface heterogeneities resulting from a polycrystalline electrode surface. The next stage of EIS studies of BMIM-OTf attempted to address the topic of the electrode surface. The next electrode used was a polished gold (1 0 0) electrode, used in previous studies by other members of our laboratory. The electrode surface was initially aligned to the (1 0 0) face to within less than 1° using back-Laue X-ray scattering patterns. Before use in experiments with RTIL electrochemistry, the validity of the

electrode was verified using a well-understood electrochemical system: a CV in 0.1M Perchloric acid [67, 68].

At this point during this project, we discovered several papers by Roling *et al* that outlined and emphasized an EIS analysis method that proved useful for identifying multiple capacitive processes. Roling's analysis method is described in Chapter 2. To recap, this analysis method involves plotting the data in the complex capacitance plane (CCP), i.e., computing an imaginary and a real capacitance for each frequency in a series and constructing a curve for each potential studied. Equation 5.1.3, shown below, gives the expression for the complex capacitance calculation.

$$C'' = \frac{1}{j(2\pi f)Z''} \tag{5.1.3}$$

Plotting EIS data in this way allows the researcher to observe features that may not have been evident in a Nyquist representation. In the CCP representation, the real portion C' corresponds to electrical energy stored by the interface, and the imaginary portion C'' corresponds to dissipated electrical energy [69]. Capacitive processes appear in the CCP as semi-circle shapes differentiated by their individual time-constants. Figure 5.6 shows a sample of our data for the Au (100) electrode and BMIM-OTf represented in the CCP.

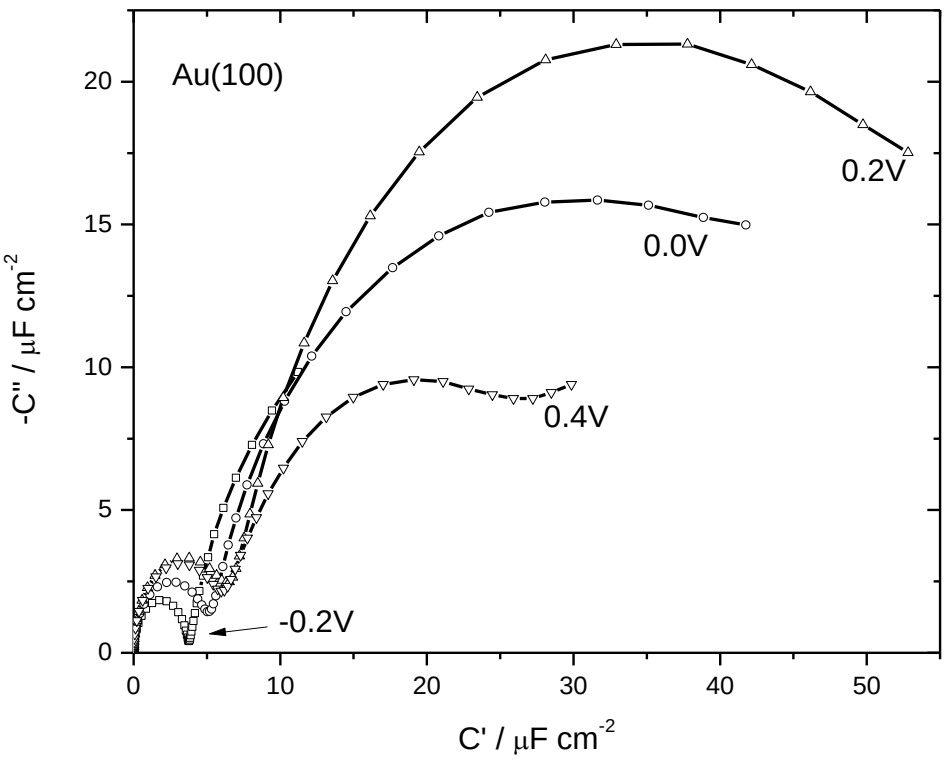

Figure 5.6 – Complex Capacitance Plane (CCP) representation of EIS data for Au(100) and BMIM-OTf

Two distinct processes are clearly visible, and one could argue that a third is apparent – particularly at the tail-end of the 0.4V curve. The existence of a third process is conjecture at best based on the data in Figure 5.6. For this reason, we have chosen to focus on the two clearly evident processes. The first, or high-frequency, semi-circle is a relatively fast process, occurring on a millisecond time-scale. Such a process can only be non-Faradaic in nature, and we assign this to the rearrangement in the double-layer region. It is important to note that the shape of this feature is not perfectly round and appears to be "squished" horizontally, indicating a deviation from a perfect capacitance. Based on the previous EIS and chronocapacity studies, this conclusion makes sense. The second process visible in the CCP data has a much slower time-constant, on the order of seconds. The slow nature of this process point toward it originating within the kinetic processes

of slow ion transport within the RTIL. The slow interfacial relaxation seen in the chronocapacity transients further supports this assignment.

5.2 Immersion Experiments - Conclusions Regarding PZC

In order to gain further insight into the nature of the structure and behaviour of the RTIL electrochemical interface, electrode immersion experiments were undertaken. The goal of these experiments was to uncover critical details regarding the location of the potential of zero charge (PZC). As outlined previously, the PZC is an important parameter to know for any electrochemical system. It provides a reference point for which the state of the surface charge of the electrode can be defined – a switching point from positive to negative charge, and vice-versa. The immersion experiments are relatively simple in theory, but proved to be quite difficult in practice.

To recap, the method begins with a setup exactly the same as all other electrochemical measurements in this project. The working electrode (set up in the hanging meniscus configuration) is prepared to ensure a clean and dry electrode surface. The electrode is placed above the surface of the RTIL in the inert environment of the cell. Before contacting the surface, a potential of interest is applied to the working electrode, followed by carefully making contact between the RTIL and electrode with the aim of making an ideal meniscus as shown in Figure 3.2(a). It may seem trivial, but the immersion event was relatively difficult as the type of electrode presented several issues in this type of setup. First, the RTIL tended to "jump" to the electrode upon contact. This jumping was troublesome because the RTIL would creep up the side of the electrode resulting in a larger than anticipated electrode area. This wicking effect introduces variability of subsequent runs and needed to be minimized. Secondly, the electrode was mounted

in a glass tube, which slid inside a Teflon adapter plug that was fitted to the cell top. Since the fit was purely frictional, sliding the glass electrode tube in a precise fashion was not easy and often resulted in deeper than intended immersion. Beyond that, the pushing action created vibrations in the entire cell assembly that could cause the RTIL to contact the electrode at an angle. The recorded current transient exhibited a strange shape when this occurred due to the RTIL contacting the surface in a non-uniform fashion. To counter these problems, we opted to take an opposite approach and bring the RTIL to the electrode. The cell was fitted with a small glass syringe at the bottom to allow manipulation of the level of RTIL in the cell. Performing the experiments with this methodology proved to be far more reproducible and we were able to achieve some favourable and interesting results.

Figure 5.7 shows an example of a transient collected at a potential clearly positive of the PZC, +500mV vs AgCl. Data collection routines were developed in-house for use with LabVIEW. Data collection was triggered by the detection of current and included a 0.25 second buffer to ensure that we did not miss the immersion event. Data collection was stopped at 1.0 seconds for consistency across each subsequent measurement. While collecting longer would have allowed the current and interface to reach equilibrium, the chronocapacity experiments showed that this would be nearing 10 minutes resulting in a very large amount of collected data. This is due to the high sampling rate required to capture the immersion event and double-layer formation.

The current spike is positive and this confirms that the potential applied is positive of the PZC. It follows that as the potential drops negative of the PZC, a negative going current transient will be seen. Not only is good information available from the direction of the transient, but we are able to integrate the area under the transient to obtain the total amount of charge passed during the

first 1 second window. The shape of the transient is also a good visual indicator of the quality of the data.

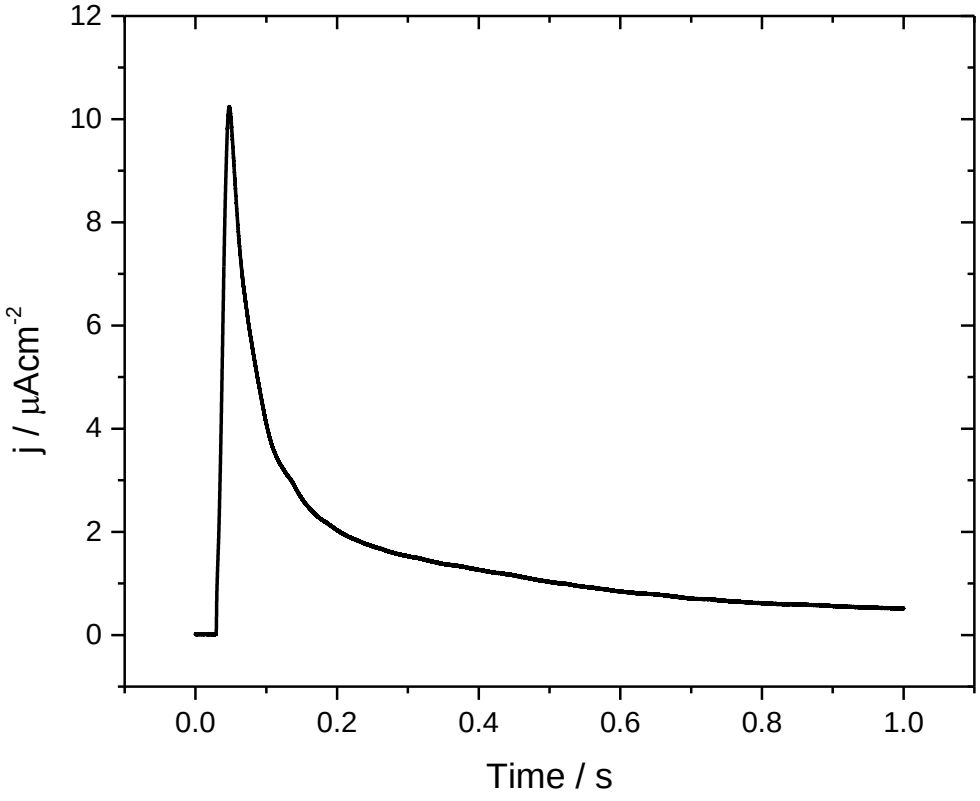

Figure 5.7 – Typical immersion transient for a potential positive of the PZC.

A transient with a shape such as shown in Figure 5.7, with a sharp peak, and smooth decay shows ideal contact was made between the RTIL and electrode with minimal sidewall creep or angled contact.

Figure 5.8a shows a plot of transients taken on the positive side of the PZC, as evidenced by the switch upward nature of the current spike. Figure 5.8b shows the transients from potentials negative of the PZC.

At this point, visual inspection of the transients is very promising. All transients have relatively sharp peaks, indicating that we are catching the fast double layer formation process. They also tend to decay as expected – in an exponential manner. It is interesting to note the scale for both the positive and negative transients. The positive transients exhibit a larger peak current, nearing the 10 $\mu A/cm^2$ mark, while the negative transients barely break the -4 $\mu A/cm^2$ level. It is difficult to comment on this observation and it is purely speculative at best, but this could be a potential indication of some of the effects described by Kornyshev and Fedorov [65, 70-73] as electrostriction and over-screening of RTILs with size asymmetry between the cation and anion. A size asymmetry would allow for a larger number of the smaller sized ion to populate the double layer region resulting in a larger current flow. More conclusive data is required to make and definitive claims regarding the exact structure of the double layer region for the BMIM-OTf | Au interface.

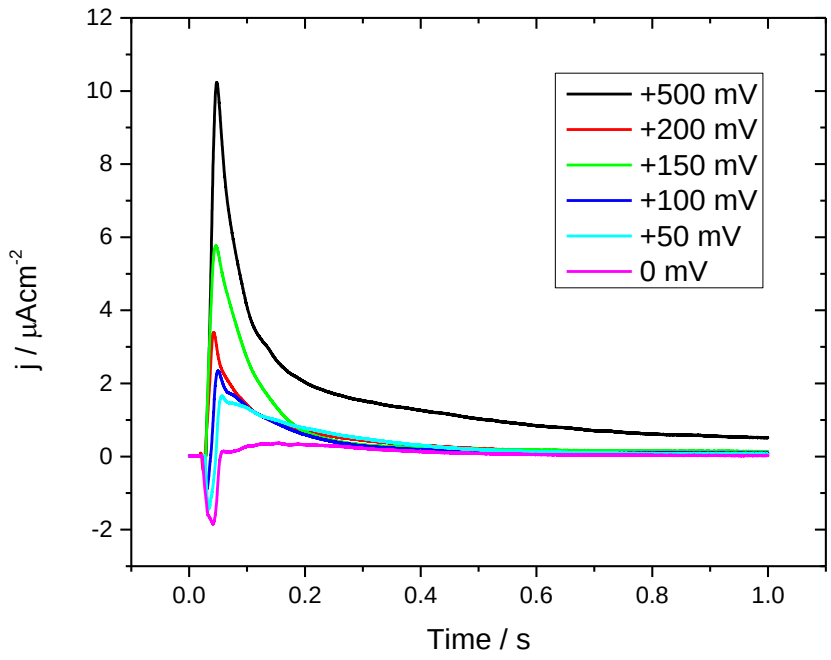

Figure 5.8a – Immersion transients showing potentials positive of the PZC.

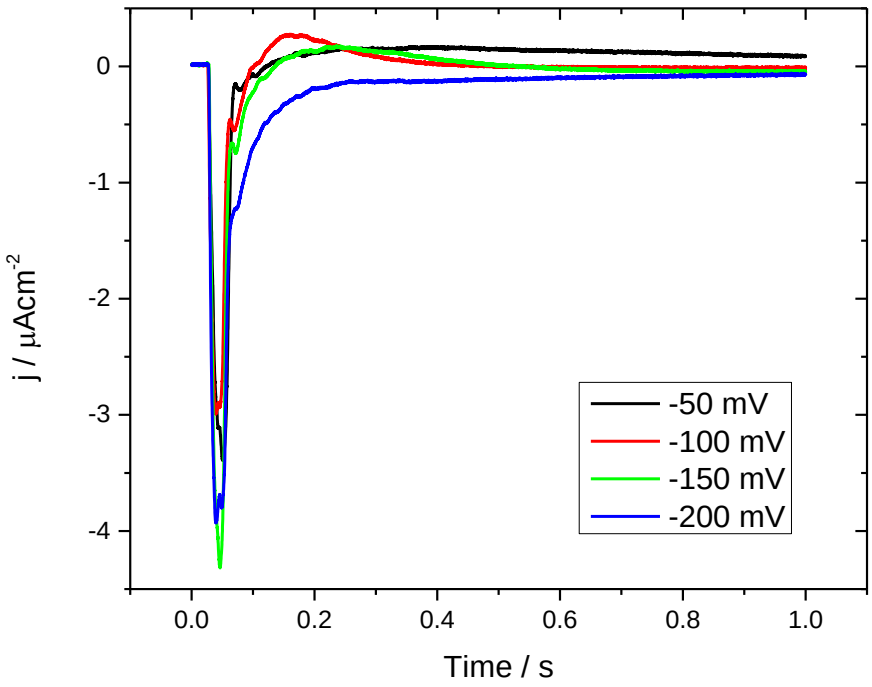

Figure 5.8b – Immersion transients showing potentials negative of the PZC.

Integration of the current-time data results in the total charge passed over the first second of double layer formation. It follows that the total charge passed will cross zero at the PZC, assuming a linear relationship. Figure 5.9 shows a plot of the total charge *versus* applied potential. Based on this plot, it can be seen that the linear trend line crosses the abscissa at approximately -70 mV vs AgCl.

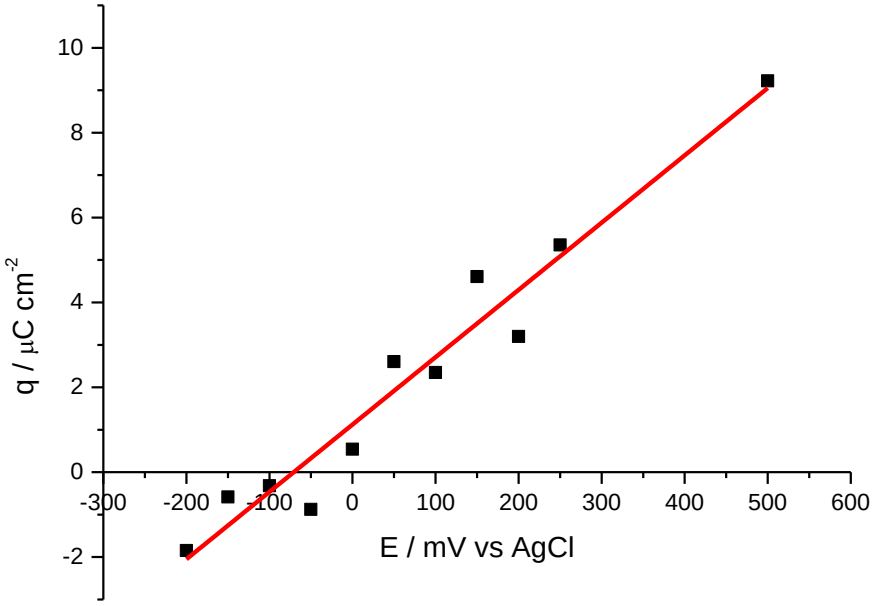

Figure 5.9 – Immersion transient integration results for PZC determination.

This is an important result, as we now have a reliable method for PZC determination in RTILs that is capable of providing some insight into this interesting interface. These results will be helpful to guide future experiments and their data analysis, as we can now characterize the interface as having excess positive or negative charge based upon where the potential is relative to the PZC.

CHAPTER 6

SUMMARY, CONCLUSIONS, AND FUTURE WORK

6.1 SUMMARY & CONCLUSIONS

The focus of the work in this thesis is on the interesting behavior of Room Temperature Ionic Liquids at electrified interfaces. Through this research we have shown that an interesting class of electrolytes possesses behavior that contradicts all contemporary electrochemical models. RTILs are interesting for this very reason, they create unique scenarios that are capable of powering research in a new direction. The work contained within this thesis is but one step towards a concerted effort to understand the electrochemistry of ionic liquids in general. This initial effort toward the systematic investigation of RTIL electrochemistry with a focus on a high level of RTIL purity has brought some interesting behavior into focus. These results have shown that high purity RTILs are capable of operating within a very wide window of potentials in a repeatable and very stable fashion.

Their hygroscopic nature presents a challenge for long term experiments, but with proper planning, handling, and a well-designed apparatus the effects of water contamination can be eliminated. Throughout the laboratory portion of this work, our approach resulted in simple improvements where our methods and electrochemical cell underwent several iterations. The design and modifications to the electrochemical cell, electrode holders, and reference electrode also consumed a sizeable fraction of the time invested in this work.

At the very basis of it all resides a high purity RTIL that was synthesized following a scheme provided by Dr. R.W.J. Scott (see Chapter 3) [35-37]. While the synthetic procedure is relatively simple, high purity product requires high purity reagents. Thus, our starting materials

needed to be freshly distilled. Following synthesis of the precursor RTIL (BMIM-Chloride) and several purification steps, an ion exchange gives the target BMIM-OTf. Again, more purification was necessary to remove any trace impurities lingering around waiting to interfere with the electrochemistry. Lastly, prior to each experiment, the RTIL had to be dried under vacuum and heat to ensure the dryness of the RTIL. As such, each milliliter of high purity BMIM-OTf was not come by easily in any sense. On the apparatus side of the experiments, the borosilicate glass cell and all of its associated parts required cleaning in a hot acid bath followed by rinsing with copious amounts of Millipore water, and drying in an oven. A similar cleaning regimen was also applied to the electrodes prior to use. While these experiments themselves may not seem to be overly difficult, the preparation required was significant and time consuming. A simple mistake had the potential of ruining several days of preparation.

Ultimately, this research pointed towards a very slow relaxation of the BMIM-OTf – electrified gold interface both upon interface formation, and changing electric potentials. The results showed a massive capacitive hysteresis that was dependent upon the initial applied electrode potential and direction of scan. This indicates that the state of the surface – whether it be anion or cation dominated – came with a steep energy cost when it came to changing electrode potentials. This effect appeared to be strongest when the potentials crossed the assumed PZC, or the potential at which the surface changes from negative to positive charge, and *vice-versa*. The significance of this may not be immediately apparent, but understanding exactly where the PZC is for systems like this is paramount to comprehending the nature of RTIL interfacial behavior. In order to ever successfully put RTILs to use in any of the proposed devices, a thorough understanding of their electrochemical behavior must be reached. Using EIS techniques in conjunction with fitting the data to a simple equivalent circuit, we were able to extract and compute

a value for the double-layer capacitance as a function of applied potential. Comparison of the shape of these experimental capacitance-potential curves to theoretical and computational work, very similar features were found. Ultimately, this allowed for a level of validation and provided strong evidence that the theoretical work was highly successful at modeling the RTIL – electrified metal interface.

Further analysis using electrochemical impedance techniques we were able to separate multiple simultaneous capacitive processes based upon their relative time-scale. These results validate the assumption that an equivalent circuit must include multiple capacitances in parallel to describe several simultaneous processes and structural rearrangements occurring at the electrode surface. Not only have we shown that we can see and separate these multiple simultaneous processes, but also that there is something to be taken from the theoretical work of others such as Kornyshev [9-13]. As mentioned previously in this thesis, the principles of lattice saturation and electrostriction, predicted by Kornyshev, do tend to strongly agree with our findings.

Finally, we attempted a series of immersion experiments aiming to draw out the elusive PZC. These experiments were based upon a technique where a potential was applied to a clean and dry electrode, followed by immersion into the RTIL and measuring the resulting current from double layer formation and arrangement relative to the applied potential. The experiments themselves were not easy to replicate, however, with some form of perseverance we were able to obtain results that were repeatable in a relative sense. With this data in hand, a simple integration reveals the total charge passed as the RTIL forms the double-layer structure upon contacting the surface of the gold electrode. Plotting this total charge *versus* applied potential nets a relatively straight trendline. The point at which this line crosses the abscissa represents zero charge passed, or the potential of zero charge, PZC. The end result of these painstakingly difficult experiments

was a PZC potential of -71mV (vs AgCl). Interestingly enough, the EIS data fitted to an equivalent circuit gives a capacity maximum at exactly the same potential! The significance and implications of these results are staggering. Given that the literature is full of experimental studies utilizing a wide variety of RTILs, methods, and electrode materials which give a wide variety of capacitance values and C-E curve shapes, this result is important. – Having an experimental study show that the PZC and capacity maximum occur at the same applied potential is great, but doing so while in agreement with the proposed computational and theoretical models is fantastic. This work provides a solid link between experiment and theory – effectively reducing the knowledge gap and bringing RTIL electrochemistry closer to the point where RTILs can be utilized to their full potential (no pun intended).

6.2 FUTURE WORK

The next steps for RTIL interfacial research need to remain focused upon high levels of RTIL purity, first and foremost. The work contained within this thesis has shown that a fundamental understanding of the RTIL|electrified metal interface requires an RTIL of the highest level of purity. Additionally, the other side of the interface is just as important, therefore a well-defined and ultra clean metal surface is required to properly and clearly define this interface on a fundamental level. Keeping control of these two variables will put an electrochemical study in a good position to achieve reliable and accurate results. The work in this thesis has shown to have the RTIL purity issue under control. The metal surface side of the interface does have room for improvement. By taking the time to develop and classify a single crystal gold electrode we can effectively remove the smearing effect seen by using polycrystalline electrodes. Having a well-

defined surface from which we can study the electrochemical behavior of RTILs will help simplify a complex situation with many variables.

As with all scientific data, interpretation is paramount. The interpretation of electrochemical data can be difficult when studying a new type of electrochemical system. Additional data from other analytical techniques that can be coupled with electrochemical methods would prove to be very useful for identifying processes seen in our impedance based studies of the RTIL interface. Several spectroscopic methods have been tied in with electrochemical approaches in so-called "spectroelectrochemistry". These are mostly limited to various methods of Infrared Absorption Spectroscopy (IRAS). Exploring this unique interface with a surface sensitive IR spectroscopic method like Surface Enhanced IRAS could provide the detailed information vital to identifying processes at this interface. Since RTILs in general tend to be based upon organic ion pairs, IRAS techniques are well suited to gathering information on the composition of the initial layers on the surface of study. By combining such surface sensitive techniques with the electrochemical methods outlined in this thesis, a second dimension is added to the electrochemical data, potentially giving information about the physical structure of the double layer region.

Initial attempts at spectroelectrochemical characterization of this surface failed. The Surface Enhanced IRAS technique utilized the Attenuated Total Reflection (ATR) mode which relies upon a Silicon hemisphere with a thin (~10nm) layer of gold deposited on its flat surface. This layer of gold becomes the working electrode and interfacial surface of study. By bouncing an IR beam through the silicon hemisphere from the spherical side, the surface is probed for structural changes while under applied potential control. The problems encountered were related to the Chemical Vapor Deposition (CVD) of Gold onto the Silicon hemisphere. Impedance measurements inherently take a significant amount of time and we found that the RTILs tended to

delaminate the Gold layer, ending the experiment. After many failed attempts, we were unable to successfully implement this specific method. A second yet similar approach that involved replacing the Silicon hemisphere with a Zinc Selenide hemisphere was found but was never attempted. Instead of plating a thin gold layer on the surface of the optical element as in the previous method, a Gold electrode is lowered onto the surface at a distance that is on the order of tens of nanometers above the surface of the ZnSe hemisphere. From this distance, the surface is probed with an IR beam bounced through the ZnSe crystal and onto the Gold surface. This should allow for strong IR signatures to be recorded, hopefully providing useful information regarding the RTIL structure on the Gold for a given applied potential. Based upon the detailed picture that these spectroelectrochemical methods can potentially provide, they merit more work and exploration in order to help verify or refute the theoretical approaches. By doing so, we can narrow the gap between the theoretical approaches and real experimental data and ultimately begin to understand and apply the electrochemical behavior of RTILs.

6.3 REFERENCES

1. Fedorov, M.V.; Kornyshev, A.A. *Chem. Rev.* **2014**, *114*, 2978.
2. Helmholtz, H. *Annalen der Physik*. **1853**, *165*, 6, 211.
3. Bard, A.J.; Faulkner, L.R. Models for Double-Layer Structure, in *Electrochemical Methods – Fundamentals and Applications*, Wiley & Sons: New York; **2001**, pp 544-554.
4. Gouy, G. *J. Phys. Radium*. **1910**, *9*, 457.
5. Gouy, G. *Compt. Rend.* **1910**, *149*, 654.
6. Chapman, D.L. *Phil. Mag.* **1913**, *25*, 475.
7. Stern, O. *Z. Electrochem*, **1924**, *30*, 508.
8. Grahame, D.C. *Chem. Rev.* **1947**, *41*, 441.
9. Kornyshev, A.A.; *J. Phys. Chem. B.* **2007**, *111*, 5545.
10. Fedorov, M.V.; Kornyshev, A.A. *Chem. Rev.* **2014**, *114*, 2978.
11. Fedorov, M.V.; Kornyshev, A.A. *J. Phys. Chem. B.* **2008**, *112*, 11868.
12. Fedorov, M.V.; Kornyshev, A.A. *Electrochim. Acta.* **2008**, *53*, 6835.
13. Fedorov, M.V.; Georgi, N.; Kornyshev, A.A. *Electrochem. Comm.* **2010**, *12*, 296.
14. Démery, V.; Dean, D.S.; Hammant, T.C.; Horgan, R.R.; Podgornik, R. *J. Chem. Phys.* **2012**, *137*, 064901.
15. Bazant, M.Z.; Storey, B.D.; Kornyshev, A.A. *Phys. Rev. Lett.* **2011**, *106*, 046102.
16. Alam, M.T.; Islam, M.; Okajima, T.; Ohsaka, T.; *Electrochem. Comm.* **2007**, *9*, 2370.

17. Alam, M.T.; Islam, M.; Okajima, T.; Ohsaka, T.; *J. Phys. Chem. C.* **2007**, *111*, 18326.

18. Alam, M.T.; Islam, M.; Okajima, T.; Ohsaka, T.; *J. Phys. Chem. C.* **2008**, *112*, 16600.

19. Alam, M.T.; Islam, M.; Okajima, T.; Ohsaka, T.; *J. Phys. Chem. C.* **2008**, *112*, 16568.

20. Islam, M.; Alam, M.T.; Okajima, T.; Ohsaka, T.; *J. Phys. Chem. C.* **2009**, *113*, 3386.

21. Alam, M.T.; Islam, M.; Okajima, T.; Ohsaka, T.; *J. Phys. Chem. C.* **2009**, *113*, 6596.

22. Alam, M.T.; Islam, M.; Okajima, T.; Ohsaka, T.; *J. Phys. Chem. C.* **2011**, *115*, 19797.

23. Lockett, V.; Sedev, R.; Ralston, J.; Horne, M.; Rodopolous, T.; *J. Phys. Chem. C.* **2008**, *112*, 7486.

24. Lockett, V.; Horne, M.; Sedev, R.; Rodopolous, T.; Ralston, J.; *Phys. Chem. Chem. Phys.* **2010**, *12*, 12499.

25. Siinor, L.; Lust, K.; Lust, E.; *Electrochem. Comm.* **2010**, *12*, 1058.

26. Siinor, L.; Lust, K.; Lust, E.; *J. Electrochem. Soc.* **2010**, *157*, F83.

27. Pajkossy, T.; Kolb, D.M.; *Electrochem. Comm.* **2011**, *13*, 284.

28. Gnahm, M.; Pajkossy, T.; Kolb, D.M.; *Electrochim. Acta.* **2010**, *55*, 6212.

29. Drüschler, M.; Huber, B.; Passerini, S.; Roling, B.; *J. Phys. Chem. C.* **2010**, *114*, 3614.

30. Drüschler, M.; Huber, B.; Roling, B.; *J. Phys. Chem. C.* **2011**, *115*, 6802.

31. Roling, B.; Drüschler, M.; Huber, B.; *Faraday Discuss.* **2011**, *154*, 303.

32. Drüschler, M.; Roling, B.; *Electrochim. Acta.* **2011,** *56*, 7243.

33. Drüschler, M.; Borisenko, N.; Wallauer, J.; Winter, C.; Huber, B.; Endres, F.; Roling, B.; *Phys. Chem. Chem. Phys.* **2012**, *14*, 5090.

34. Atkin, R.; Borisenko, N.; Druschler, M.; El Abedin, S.Z.; Endres, F.; Hayes, R.; Huber, B.; Roling, B.; *Phys. Chem. Chem. Phys.* **2011**, *13*, 6849.

35. Dash, P.; Dehm, N.A.; Scott, R.W.J. *J. Mol. Catal. A: Chem*. **2008**, *286*, 114-119.

36. Huddleston, J.G.; Visser, A.E.; Reichert, W.M.; Willauer, H.D.; Broker, G.A.; Rogers, R.D. *Green Chem*. **2001**, 156-164.

37. Dash, P.; Scott, R.W.J. *Chem. Comm.* **2009**, *7*, 812-814.

38. Lasia, A. Electrochemical Impedance Spectroscopy and Its Applications. In *Modern Aspects of Electrochemistry 32*; Conway, B.E., Bockris, J.O'M., White, R.E., Ed.; Kluwer Academic Publishers: New York, **1999**, pp 143-248.

39. Drüschler, M.; Huber, B.; Roling, B. *J. Phys. Chem. C*. **2011**, *115*, 6802-6808.

40. Czajkowski, J.M.; Blaszczyk, T.; Kazmierczak, D. *Electrochim. Acta*. **1984**, *29*, 439-443.

41. Huber, B.; Roling, B. *Electrochim. Acta*. **2011**, *56*, 6569-6572.

42. Fafilek, G. *Solid State Ionics*. **2005,** *176*, 2023-2029.

43. A.A. Kornyshev, *J. Phys. Chem. B,* **2007**, *111*, 5545.

44. Oldham, K.B. *J. Electroanal. Chem.,* **2008**, *613*, 131.

45. M.V. Fedorov, A.A. Kornyshev, *J. Phys. Chem. B,* **2008**, *112*, 11868.

46. M.V. Fedorov, A.A. Kornyshev, *Electrochim. Acta*, **2008**, *53*, 6835.

47. M.V. Fedorov, N. Georgi, A.A. Kornyshev, *Electrochem. Comm.*, **2010**, *12*, 296.

48. M.T. Alam, M. Islam, T. Okajima, T. Ohsaka, *Electrochem. Comm.*, **2007**, *9*, 2370.

49. M.T. Alam, M. Islam, T. Okajima, T. Ohsaka, *J. Phys. Chem. C*, **2008**, *112*, 16600.

50. M. Islam, M.T. Alam, T. Ohsaka, *J. Phys. Chem. C*, **2008**, *112*, 16568.

51. S. Baldelli, *J. Phys. Chem. B*, **2005**, *109*, 13049.

52. L. Siinor, K. Lust, E. Lust, *Electrochem. Comm.*, **2010**, *12*, 1058.

53. M. Gnahm, T. Pajkossy, D.M. Kolb, *Electrochim. Acta*, **2010**, *55*, 6212.

54. Y.Z. Su, Y.-C. Fu, J.-W. Yan, Z.-B. Chen, B.-W. Mao, *Angew. Chem. Int. Ed. Engl.*, **2009**, *48*, 5148

55. M.T. Alam, M. Islam, T. Okajima, T. Ohsaka, *J. Phys. Chem. C*, **2007**, *111*, 18326.

56. C. Nanjundiah, *J. Electrochem. Soc.*, **1997**, *144*, 3392.

57. M.T. Alam, M. Islam, T. Okajima, T. Ohsaka, *J. Phys. Chem. C*, **2009**, *113*, 6596.

58. V. Lockett, R. Sedev, J. Ralston, M. Horne, T. Rodopolous, *J. Phys. Chem. C*, **2008**, *112*, 7486.

59. L. Siinor, K. Lust, E. Lust, *ECS Trans.*, **2009**, *16*, 559.

60. J.G. Huddleston, A.E. Visser, W.M. Reichert, H.D. Willauer, G.A. Broker, R.D. Rogers, *Green Chem.*, **2001**, *3*, 156.

61. N. Nanbu, Y. Sasaki, F. Kitamura, *Electrochem. Comm.*, **2003**, *5*, 383.

62. Orazem, M.; Tribollet, B. Time Constant Dispersion, In *Electrochemical Impedance Spectroscopy*; Wiley & Sons: New Jersey; **2008**; pp 233-237.
63. Gnahm, M.; Pajkossy, T.; Kolb, D.M. *Electrochim. Acta*. **2010**, *55*, 6212-6217.
64. Barsoukov, E.; MacDonald, J.R. *Impedance Spectroscopy: Theory, Experiment and Applications*, 2nd ed.; Wiley-Interscience: Hoboken, New Jersey, **2005**.
65. Fedorov, M.V.; Kornyshev, A.A. *J. Phys. Chem. B*. **2008**, *112*, 11868-11872.
66. Murakami, A.; Nakamura, S. *J. Electrochem. Soc.* **2002**, *149*, A1385-A1388.
67. Strbac, S.; Adzic, R.R.; Hamelin, A. *J. Electroanal. Chem.* **1988**, *249*, 291-310.
68. A. Hamelin, M.J. Weaver, *J. Electroanal. Chem.* **1986**, *209*, 109-124.
69. R. Atkin, N. Borisenko, M. Drüschler, S.Z. El Abedin, F. Endres, R. Hayes, B. Huber, B. Roling, *Phys. Chem. Chem. Phys.* **2011**, *13*, 6849-6857.
70. Kornyshev, A.A. *J. Phys. Chem. B.* **2007**, *111*, 5545-5557.
71. Fedorov, M.V.; Kornyshev, A.A. *Electrochim. Acta.* **2008**, *53*, 6835-6840.
72. Fedorov, M.V.; Georgi, N.; Kornyshev, A.A. *Electrochem. Comm.* **2010**, *12*, 296-299.
73. Georgi, N.; Kornyshev, A.A.; Fedorov, M.V. *J. Electroanal. Chem.* **2010**, *649*, 261-267.
74. *Schematic model of the EDL*. (no date). Retrieved June 11, 2014 from: http://what-when-how.com/nanoscience-and-nanotechnology/electrical-double-layer-formation-part-1-nanotechnology/